Special Publication 15, pp. 539–557

Chapter 28

Eagle's Nest: A Magmatic Ni-Sulfide Deposit in the James Bay Lowlands, Ontario, Canada

James E Mungall,[†,1,2] John D Harvey,[2] Steven J Balch,[3] Bronwyn Azar[1,2] James Atkinson,[2] and Michael A Hamilton[1]

[1] *Department of Geology, University of Toronto, 22 Russell St, Toronto, Ontario, Canada M5S 3B1*

[2] *Noront Resources Ltd, 105 Adelaide St West, Ste 110, Toronto, Ontario, Canada M5H 1P9*

[3] *Canadian Mining Geophysics Ltd, 11500 Fifth Ln, Rockwood, Ontario, Canada N0B 2K0*

Abstract

The Eagle's Nest Ni-Cu-PGE deposit was discovered in the McFaulds Lake area of the James Bay lowlands of northern Ontario, Canada, in 2007 by Noront Resources Ltd. It is a magmatic sulfide deposit hosted by mafic and ultramafic rocks interpreted to be a feeder conduit beneath an extensive complex of sills and related volcanic rocks, which range in composition from dunite through ferrogabbro to rhyolite. The complex, called the Ring of Fire, has been dated at 2734.5 ± 1.0 Ma and it was emplaced into 2773.37 ± 0.9 Ma felsic plutonic rocks. The felsic rocks form a sill complex structurally beneath metasedimentary and metavolcanic rocks considered to have formed along a passive margin at ca. 2800 Ma within the Oxford-Stull domain of the North Caribou superterrane in the Archean Superior province.

In its original configuration, the Eagle's Nest deposit formed in a shallowly plunging or subhorizontal keel structure at the base of a dike-like chonolith, but subsequent deformation has turned it into a vertically plunging rod of sulfide mineralization along the northwestern margin of a north-south–striking dike.

The most magnesian chilled margin is a picrite with MgO content near 18 wt percent, placing it at the boundary between komatiite sensu stricto and komatiitic basalt. Modeling suggests that the parental magma contained at least 22 percent MgO and was derived from previously melt depleted mantle. Sulfide saturation was attained following extensive contamination of the magma, resulting in the accumulation of a slurry of olivine crystals with variable amounts of interstitial sulfide melt and postcumulus orthopyroxene at the base of the conduit, locally producing significant pools of massive sulfide at or near the lower contact. The sulfide segregation occurred at moderate degrees of sulfide supersaturation from a magma rich in chalcophile elements, leading to high base and precious metal tenors in the resulting deposit. Minor fractionation of the sulfide magma is evidenced by the dispersion of massive and net-textured sulfide compositions along a tie-line between Ni-rich monosulfide and Cu-rich intermediate sulfide solid solutions, as well as by minor quantities of vein-hosted massive sulfide with extremely enriched base and precious metal tenors throughout the deposit. The former are interpreted as sulfide cumulates, whereas the latter are possible remnants of highly evolved sulfide liquids. Extensive metamorphic remobilization of Pt is considered to be responsible for wholesale depletion of Pt in much of the massive sulfide and for the local generation of sulfide veins carrying >1,100 ppm Pt.

Introduction

The Eagle's Nest Ni-Cu-PGE deposit is an accumulation of magmatic sulfide that was discovered by Noront Resources Ltd in August 2007. As of August 2010, a mineral resource had been delimited within 1,100 m of the surface with 6.9 Mt of indicated resources grading 2.04 percent Ni, 0.95 percent Cu, 1.3 ppm Pt, and 3.4 ppm Pd, with a further inferred resource of 4.3 Mt grading 1.42 percent Ni, 0.87 percent Cu, 0.8 ppm Pt, and 3.4 ppm Pd (Golder Associates, 2010).

The Eagle's Nest deposit is located in the McFaulds Lake greenstone belt in the James Bay lowlands of northern Ontario at 52°45' N latitude and 86°17' W longitude. It is about 525 km north-northeast of the city of Thunder Bay, and about 263 km west of the community of Attawapiskat on James Bay. The surrounding landscape is a poorly drained peneplain, which slopes gently (0.7 m/km) from approximately 150 m above sea level in the property area toward James Bay and Hudson's Bay to the east and northeast, respectively. The terrain is flat and swampy, generally covered by string bogs and muskeg.

[†] Corresponding author: e-mail, mungall@geology.utoronto.ca

Bedrock in the deposit area belongs to the Oxford-Stull domain of the North Caribou superterrane of the Archean Superior province and is locally overlain by Paleozoic sandstone and platform carbonate of the James Bay lowlands. The trace of the unconformity is highly irregular in plan and is obscured by a regionally extensive sheet of glacial tills, gravels, marine clays, and peat deposited during and after the Pleistocene glaciations. A few isolated outcrops of Archean rocks are found along stream channels in the region, where they project through the Paleozoic cover and have been exposed by incision of the streams. An extensive saprolitic regolith remains beneath the Paleozoic sedimentary rocks, locally reaching depths greater than 50 m below the unconformity.

Exploration History

Little surface geological work has been done in the McFaulds Lake region. The first geological investigations in the region were conducted by the Geological Survey of Canada as part of the "Roads to Resources" program between 1960 and 1962. The Lansdowne House map (Bostok, 1962) and accompanying summary report (Duffell et al., 1963) resulted

from this work and cover the NTS map sheet 43D which covers the deposit. No further field mapping has ever been conducted in the deposit area, although there have been some subsequent regional compilation projects which have recycled the original outcrop observations acquired by Bostok in 1961. The Ontario Department of Mines conducted a helicopter-supported mapping project in the area (Bennett and Riley, 1969). The results of all of these studies were compiled by Thurston et al. (1979).

Diamond exploration began in the region in 1959 and continued sporadically until the discovery of diamondiferous kimberlites by Monopros Ltd. in 1988. In April 2002, drilling of an isolated magnetic anomaly in search of kimberlite by Spider Resources Inc. led to the discovery of the McFaulds VMS deposits. The discovery prompted the recognition of the region as a poorly exposed greenstone belt that was highly prospective for further discoveries of base metal deposits. Subsequent discoveries have included six other VMS deposits in the McFaulds group, and others about 20 km to the west and several tens of kilometers to the north.

In August 2007, Noront Resources Ltd drilled a hole in a short, strike-limited coincident magnetic and conductive anomaly searching for more VMS deposits, but instead discovered tens of meters of disseminated to net-textured magmatic Ni-Cu-PGE-Fe sulfide mineralization hosted by metaperidotite. By the time that the fifth hole was completed a few days later, the Eagle One deposit was known to contain a highly significant zone of magmatic massive sulfide mineralization. Subsequent drilling to depths greater than 1,000 m led to discoveries of more lenses of massive sulfide and the deposit was renamed Eagle's Nest.

Since that time, follow-up anomaly testing in the region by Noront and other junior companies has uncovered the Eagle Two and AT12 magmatic massive sulfide deposits and the Blackbird, Big Daddy, Black Thor, and Black Label chromitite deposits within the same ultramafic rocks of the Ring of Fire complex that host the Eagle"s Nest deposit.

Regional and Local Geology

Superior province

The McFaulds Lake area is underlain by Precambrian rocks of the northwestern part of the Archean Superior province. The Superior province forms the nucleus of the Canadian Shield and is the world's largest contiguous exposed Archean craton. The northwestern part of the Superior province (shown in Fig. 1) is composed of a series of major Mesoarchean volcanic and plutonic belts, which each trend east-west and formed as separate microcontinents ca. 3.0 Ga (e.g., Percival et al., 2006); they are now separated by younger Neoarchean metasedimentary belts and crustal-scale faults. These oceanic microcontinents or terranes were amalgamated to form the current architecture of the Superior province.

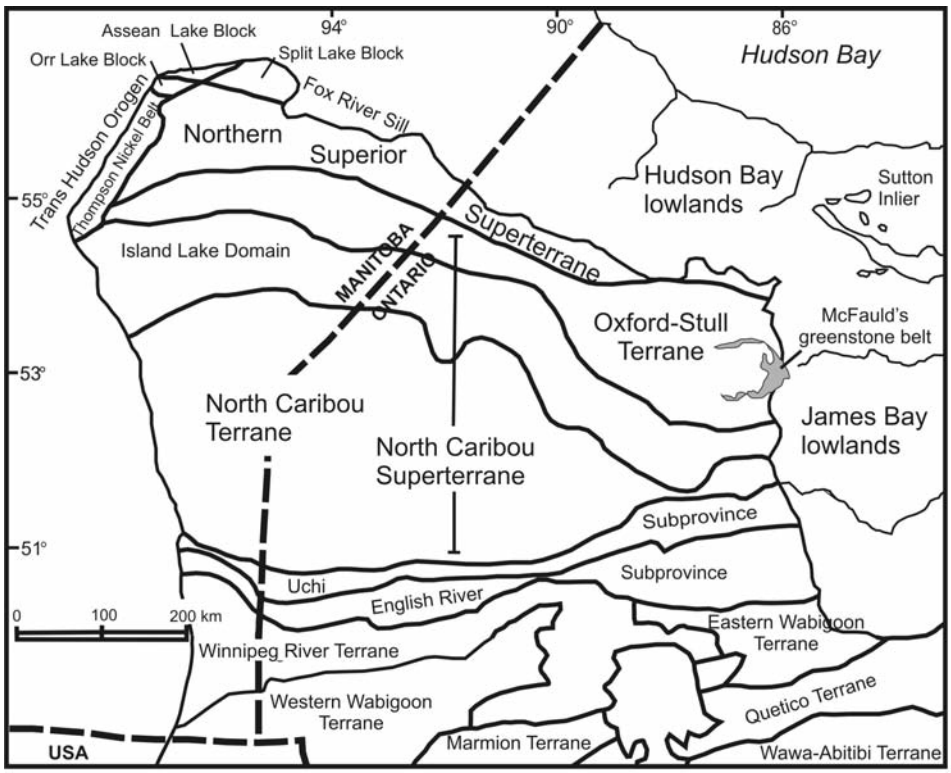

FIG. 1. Tectonic map of northwestern Ontario (after Rayner and Stott 2005). The terranes shown comprise the northwestern part of the Superior province, which is overlain to the north, west, and east by Paleozoic sedimentary rocks. To the northwest it is bounded by Paleoproterozoic rocks of the Trans-Hudson orogen. The McFaulds Lake greenstone belt occupies the southern half of the extreme eastern limit of the Oxford-Stull terrane, where it disappears beneath Paleozoic cover in the James Bay lowlands.

The McFaulds Lake area lies within a domain of the Superior province formerly called the Sachigo subprovince, but later renamed the North Caribou superterrane (Rayner and Stott, 2005; Percival et al., 2006) (Fig. 1). The core of the North Caribou superterrane is the North Caribou terrane, a series of >3.0 Ga volcanic, metasedimentary, and plutonic rocks that underwent repeated episodes of deformation and plutonism between 3.0 and 2.7 Ga (Percival et al., 2006). Around the margins of the North Caribou terrane, there are remnants of a platformal sedimentary succession comprising quartzite, arkose, and iron formation thought to have formed during a rifting event at ca. 2990 Ma. The rift succession is locally overlain by mafic to komatiitic lavas.

Subsequent to the rifting event, subduction along the northern and southern margins of the North Caribou terrane led to episodes of arc volcanism, sedimentation, and accretion of fragments of intraoceanic island arcs, and was also associated with some obduction of oceanic crust. The largely juvenile crust accreted onto the margins of the North Caribou terrane is defined as the Island Lake domain on its north margin and the Uchi domain (formerly Uchi subprovince) on its south margin.

The Oxford-Stull domain (Thurston et al., 1991; Oxford-Stull subprovince of Rayner and Stott, 2005), which contains the McFaulds Lake greenstone belt, trends east-southeast along the northern margin of the North Caribou terrane, from northwestern Manitoba to north-central Ontario, where it then extends under the Paleozoic cover rocks of the James Bay lowlands. It is distinguished from the North Caribou terrane by its lack of pre-3.0 Ga crustal age as determined by U-Pb dating or Sm-Nd isotope systematics. Its southern boundary is a series of major ductile shear zones, which separate it from the other parts of the North Caribou superterrane.

McFaulds Lake greenstone belt

The detailed tectonic history of the McFaulds Lake greenstone belt has yet to be determined. As recently as 1999 (Percival et al., 1999), no greenstone belt was recognized in the area because of the near-total absence of outcrops of supracrustal rocks. The discovery of the McFaulds Lake VMS deposits in 2003 attracted attention to the area and it is now recognized that a significant greenstone belt exists at the eastern limit of exposure of the Oxford-Stull domain, near where it disappears under the Paleozoic cover.

The oldest known rock within 100 km of McFaulds Lake is a tonalite to granodiorite gneiss emplaced at 2813 ± 4 (Rayner and Stott, 2005). Seven other plutonic rocks from within the Oxford-Stull domain, also dated by Rayner and Stott (2005), range in age from 2727 to 2683 Ma. Some of the rocks contain inherited zircon cores that are as old as 2886 Ma, consistent with the apparent crust-formation ages of 2.95 to 2.7 Ga. A sample of intermediate volcanic rock from drill core at the McFaulds Lake VMS deposits gave a U-Pb age of 2737 Ma and a crust-formation age of 2.84 Ga.

Knowledge of the local geology in the McFaulds Lake greenstone belt is constrained almost exclusively through airborne geophysical surveys and diamond drilling, both motivated by exploration for diamonds and base and precious metals. Outcrops are scarce, being concentrated mostly along stream channels that have scoured down through Pleistocene overburden. Outcrops are almost exclusively erosion-resistant granitoids, even in areas known from diamond drilling to contain abundant supracrustal sequences.

The most useful data at the regional scale are the airborne magnetometer survey results compiled in Figure 2a. A key feature of this image is the formational magnetic high, which forms a lineament in the shape of a half-circle 60 km in diameter in the middle of the figure. This feature was named the Ring of Fire early in the exploration history of the area in recognition of its proximity to several newly discovered mineral deposits, including the McFaulds Lake VMS deposits and the Eagle's Nest and Eagle Two magmatic sulfide deposits. Numerous diamond drill hole intersections of the lineament show that the high magnetic susceptibility is, in most cases, produced by the presence of silicate- and oxide-facies iron formation, which locally contains highly conductive pyrrhotite laminae. The iron formation is interpreted to young outward from the lineament, based on such features as layering in ultramafic-mafic sills and the settling of magmatic sulfides within ultramafic intrusions, as well as a contrast in metamorphic grade across lineament. This prominent marker horizon separates older, highly deformed rocks with upper amphibolite facies mineral assemblages within the lineament from younger rocks outside the lineament that show relatively simple aeromagnetic fabric indicative of a simpler deformational history. These younger rocks have an upper greenschist to lower amphibolite facies mineralogy.

The preponderance in outcrop of felsic intrusive rocks within the lineament has led to its historical classification as a purely plutonic domain. Recently, at least five different VMS deposits have been discovered through diamond drilling in the area. These, combined with proprietary high quality airborne geophysical data, make it clear that this region is made up of a complexly folded and refolded package of supracrustal metasedimentary and metavolcanic rocks whose volume has been tremendously inflated by younger felsic intrusions.

Far from the iron formation and the mineral deposits, where diamond drilling has been more limited, it is difficult to interpret the aeromagnetic fabric with any confidence. A plausible interpretation of the information available to date is that the crust inside the ring and other similar domal bodies is the oldest crust in the region (Fig. 2b). These bodies, volumetrically dominated by felsic plutonic rocks in the McFaulds Lake region, were formed ca. 2.95 to 2.85 Ga as an amalgamation of juvenile volcanic rocks, sediments, and coeval plutons in an intraoceanic island arc (e.g., Percival et al., 2006). These subsequently underwent deformation, perhaps during accretion onto the North Caribou superterrane, and, following a period of erosion, were covered by a regionally extensive iron formation which forms much of the magnetic lineament originally dubbed the Ring of Fire. This was covered, in turn, by a clastic sedimentary and volcanic package (the McFaulds Lake greenstone belt; Fig 2b).

At some time after the deposition of the iron formation, a major episode of ultramafic, mafic, and intermediate to felsic magmatism occurred. This intrusive suite consists of peridotitic to dunitic dikes and sills, as well as a layered intrusion of leucogabbro, anorthosite, and ferrogabbro which directly underlies a pile of intermediate to felsic lavas and pyroclastics intruded by ferrogabbro sills (Figs. 2b, 3). The Big Mac complex probably belongs to the same suite (Fig. 2b), however

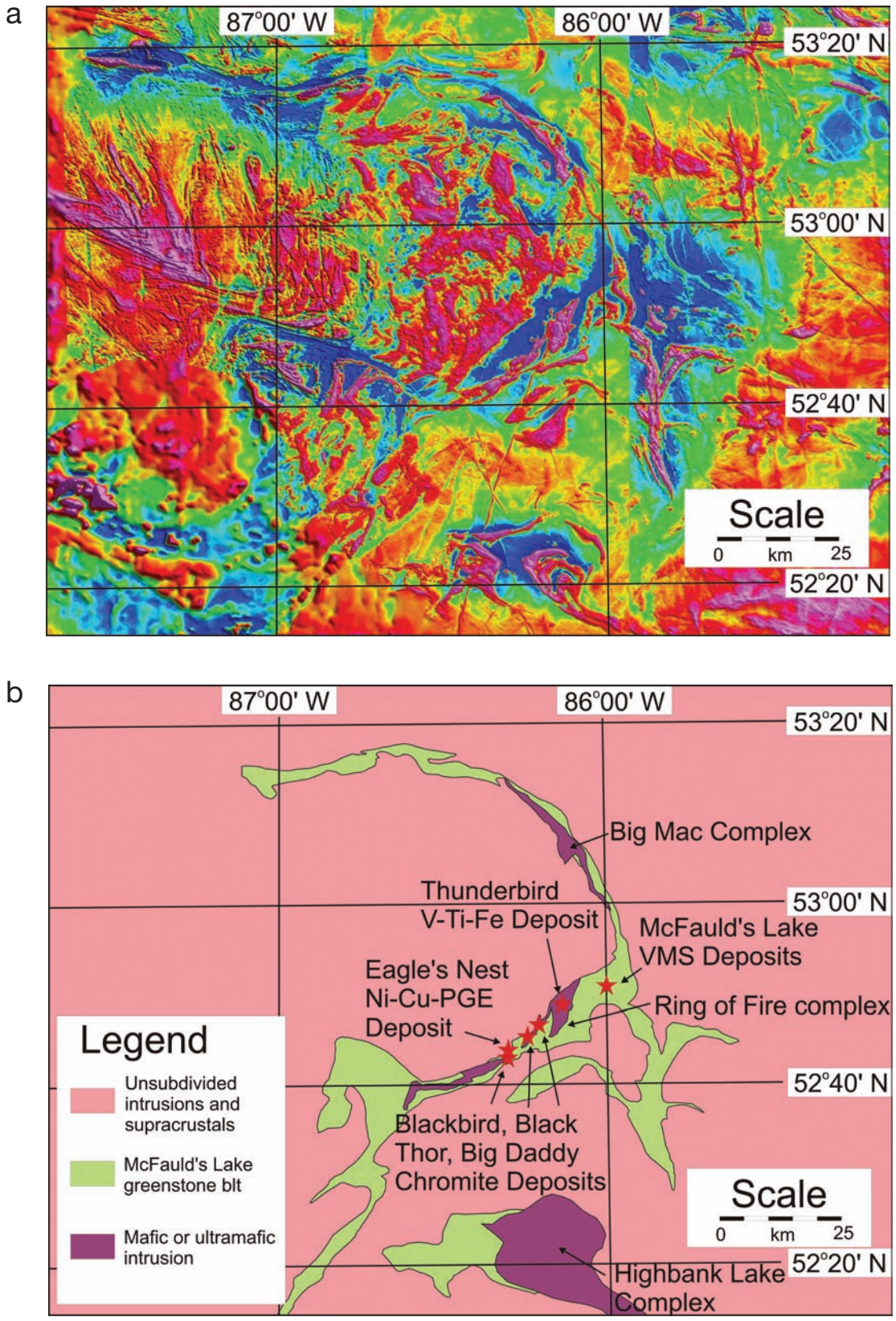

FIG. 2. a. Aeromagnetic map of the Ring of Fire region. The prominent near-circular pattern in the middle of the figure is the lineament that was originally called the Ring of Fire. b. Geological sketch map indicating the inferred extent of gneiss domes with Mesoarchean crust formation ages (pink), Neoarchean greenstones (green), and the Ring of Fire ultramafic-mafic complex and related intrusions including the Big Mac and Highbank Lake complexes (purple).

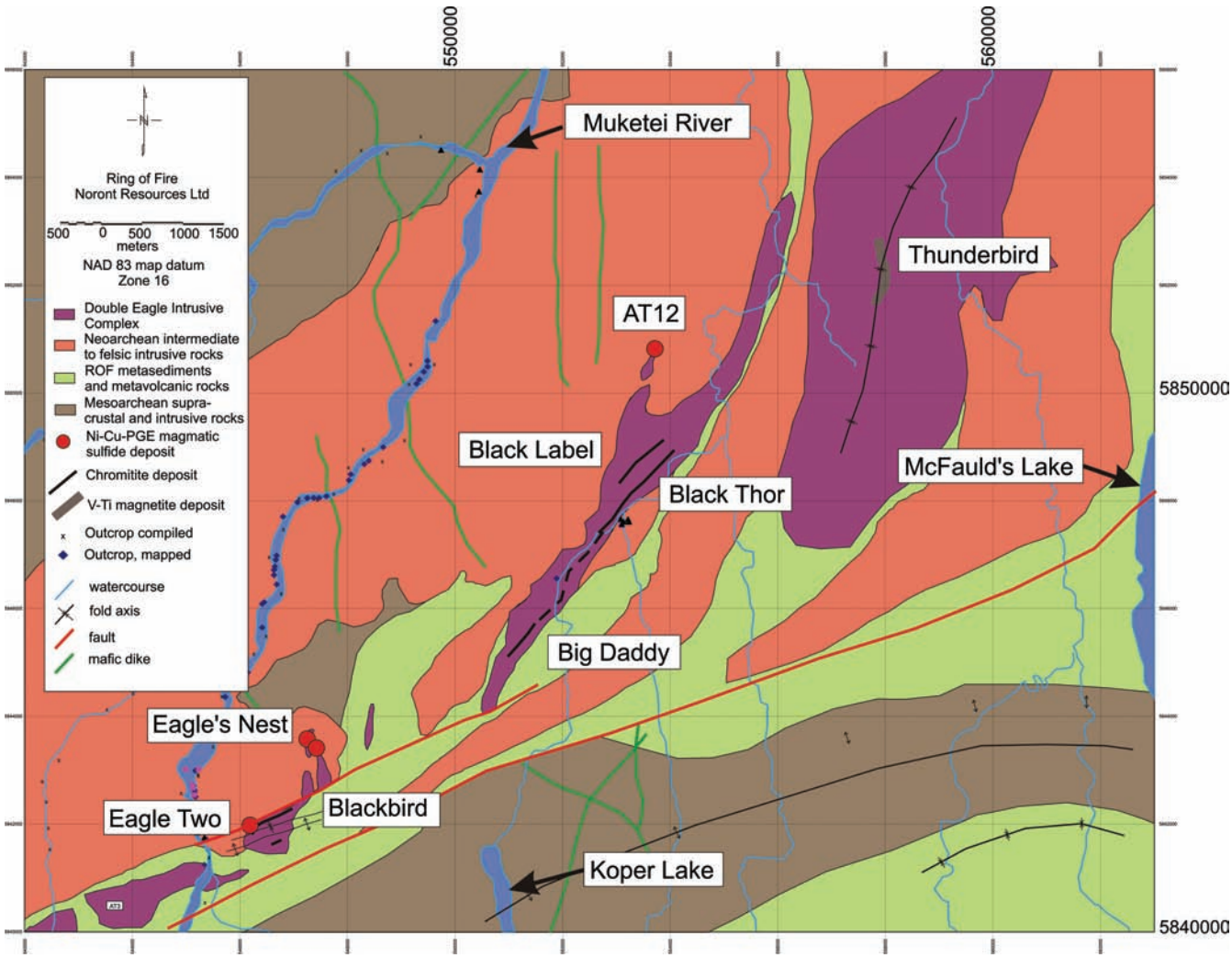

FIG. 3. Geological sketch map of the presumed geology of the area surrounding the Ring of Fire Complex, based on numerous exploration drill holes and the magnetic fabric shown in Figure 2.

the Highbank Lake complex to the south is considered to be older (G. Stott, pers. commun., 2009). The entire suite of dikes, sills, layered intrusion, and felsic volcanic rocks can be collectively termed the Ring of Fire complex.

The magnetic fabric shown in Figure 2a allows the area to be divided into several zones with different geophysical responses, which are discussed here with reference to the geological sketch map of the area surrounding the known mineral deposits in Figure 3. The northwestern edge of the map shows a mottled moderate magnetic response. It is inferred to be the basement gneiss complex comprising discontinuous, but locally magnetite-rich metasedimentary rocks and abundant intermediate to felsic intrusions, which also contain variable amounts of magnetite.

Southeastward of the gneiss dome a broad zone of muted magnetic response and subtle northeast to southwest lineaments defines a stacked series of felsic intrusions, which are similar to the granodiorite that hosts the Eagle's Nest deposit. Along the southeastern margin of the magnetic quiet zone is a string of highly magnetic bodies, several of which contain bedrock conductors, which are dike-like intrusions of ultramafic rock. These appear both as isolated bodies surrounded by granodiorite, as at Eagle's Nest, and as more extensive sheets along a lineament spanning the entire belt. Immediately south and east of this belt of ultramafic and mafic intrusions, there is a second string of highly magnetic rocks that also show local bedrock conductivity due to the presence of iron formations. Ultramafic sill-like intrusions above the dikes were preferentially developed at the horizon formerly occupied by the iron formation, which has been replaced by extensive layered sills of dunite, harzburgite, orthopyroxenite, and chromitite, probably in part through a process of magmatic assimilation. The Blackbird, Big Daddy, Black Label, and Black Thor chromitite deposits are hosted by these ultramafic sills.

In the far northeast of Figure 3, there is a prominent highly magnetic structure suggesting concentric layers of alternating high and very high magnetic susceptibility. This structure was drill-tested in early 2009 in its most magnetic portions to reveal interlayered anorthosite and magnetite-rich ferrogabbro containing numerous ductile shear zones, indicating that this is a tectonically disrupted layered intrusion. The area underlying

the highest total magnetic field is made up of a mass of magnetite-rich gabbro, several hundred meters thick, which has been drill-tested over more than 1 km of strike length and is called the Thunderbird V-Ti-Fe deposit. It is possible to trace similar highly magnetic ferrogabbros in the aeromagnetic pattern continuously from the chromitite-bearing ultramafic sills, where they have been observed to overlie the chromitite, to the base of the layered intrusion. Ferrogabbro sills hosted by felsic volcanic rocks have also been encountered in drill core immediately beneath the McFaulds Lake VMS deposits just east of the map area in Figure 3.

Subsequent, and as yet undated, igneous activity in the region included the intrusion of a suite of late- to posttectonic leucogranites and rare element-rich pegmatites into all of the above rock units. Shortly following the intrusion of the Ring of Fire complex, the region underwent a protracted episode of arc plutonism, which continued at least until 2690 Ma (Rayner and Stott, 2005). The current dome-and-basin structure, with uplifted volcano-plutonic massifs surrounding synclinal keels of younger greenstones, is typical of Archean greenstone belts and probably formed during a compressional stage associated with accretion of the Northern Superior superterrane onto the North Caribou superterrane ca. 2720 Ma (Percival et al., 2006).

Geochronology of the Ring of Fire Complex

Two samples from the Ring of Fire complex have been dated by U-Pb analyses of zircon. They are reported here to place the intrusive event in a geological context.

One sample, NOT-07-06-a, is tonalite host rock of the Eagle's Nest deposit taken about 50 m outside the ultramafic contact. It is a medium-grained, equigranular tonalite which comprises centimeter-scale, strongly zoned plagioclase phenocrysts surrounded by a matrix of plagioclase, quartz, biotite, and hornblende. The tonalite has undergone minor alteration to epidote, clinozoisite, chlorite, and tremolite, but retains much of its primary mineral assemblage. Locally, the tonalite shows strong metamorphic fabrics, with a strong lineation within a somewhat weaker plane of foliation typically developed close to major lithotectonic boundaries, such as the contact with the Ring of Fire complex.

The second sample, NOT-08-2G17-a, is a ferrogabbro from the Ring of Fire complex about 12 km east of the Eagle's Nest deposit. This ferrogabbro is composed of actinolite, chlorite, clinozoisite, plagioclase, apatite, magnetite, and ilmenite, with accessory zircon, after a primary assemblage of clinopyroxene, magnetite, apatite, and plagioclase. The sample was taken from a ferrogabbroic layer within a layered sequence, several hundred meters thick, comprising metadunite, chromitite of the Black Thor deposit, orthopyroxenite, leucogabbro, and ferrogabbro, all located stratigraphically and structurally on top of the AT12 feeder dike (Fig. 3), a mineralized peridotitic body very closely resembling the Eagle's Nest dike.

Zircon grains were isolated by crushing samples in a jaw crusher and disk mill, followed by using a Wilfley table for initial mineral separation. After sieving to pass 70 mesh, the heavier, nonmagnetic mineral fractions were concentrated using free-fall magnetic separation, heavy liquid flotation, and a Frantz isodynamic magnetic separator. Zircon grains were handpicked from the remaining non-magnetic fraction and treated by abrasion using pyrite (Krogh, 1982), before being annealed at 1,000°C for 48 hours prior to leaching in HF for a few hours to remove radiation-damaged portions of the crystals. Three zircon grains from each sample were dissolved in the presence of a mixed ^{205}Pb-^{235}U spike in HF in teflon bombs (Krogh, 1973). Lead and U were precipitated from the resulting solutions in anion exchange columns, using HCl and H_2O, before being loaded on Re filaments using a silica gel. Isotopic analysis was carried out using a VG354 mass spectrometer with a Daly collector in pulse-counting mode. Isotopic results are presented in Table A1 of the Appendix.

The age of the tonalitic host rock is 2773.37 ± 0.9 Ma (Fig. 4), consistent with its apparent emplacement well after the formation of the high-grade, polydeformed core of the Ring of Fire dome and perhaps also subsequent to deposition of the overlying iron formation. This age is considered to be typical of all the felsic intrusions spanning the entire strike length from the Eagle's Nest deposit, under the Blackbird, Big Daddy, Black Thor, and Black Label chromitite deposits, and past the AT12 magmatic sulfide occurrence. This is because the host rocks underlying all of these occurrences are visually indistinguishable from the dated sample and because the aeromagnetic fabric throughout this region indicates that the Ring of Fire complex here is underlain by a single fairly homogeneous felsic intrusive massif.

As shown in the concordia diagram in Figure 5, the age of the ferrogabbro sample from the Ring of Fire complex is 2734.5 ± 1.0 Ma. This age is not only consistent with its cross-cutting relations with the older host tonalite massif, but is also identical, within error, to the age of metavolcanic rocks hosting the McFaulds Lake VMS deposits and dated by Rayner and Stott (2005) at 2737 ± 7 Ma.

Understanding of the full implications of these ages for the relative timing and geodynamic significance of the Ring of Fire complex must await further geochronological work. However, it is evident that the Ring of Fire complex was coeval with the effusion of the stack of volcanic rocks that host

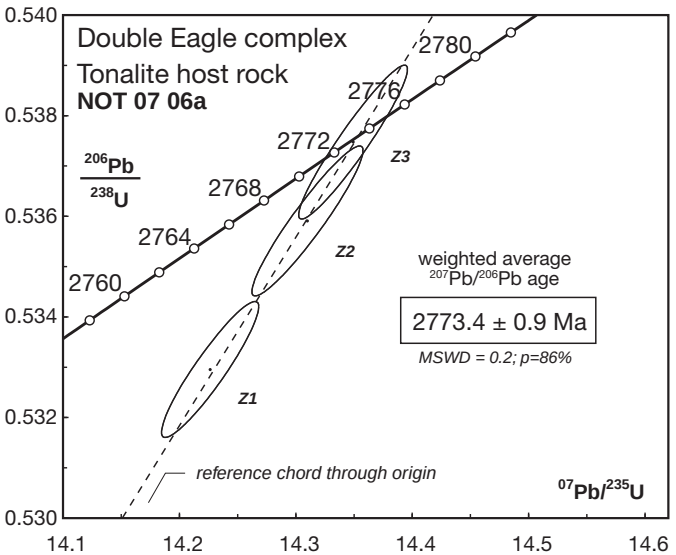

FIG. 4. Concordia diagram for sample NOT-07-06-a.

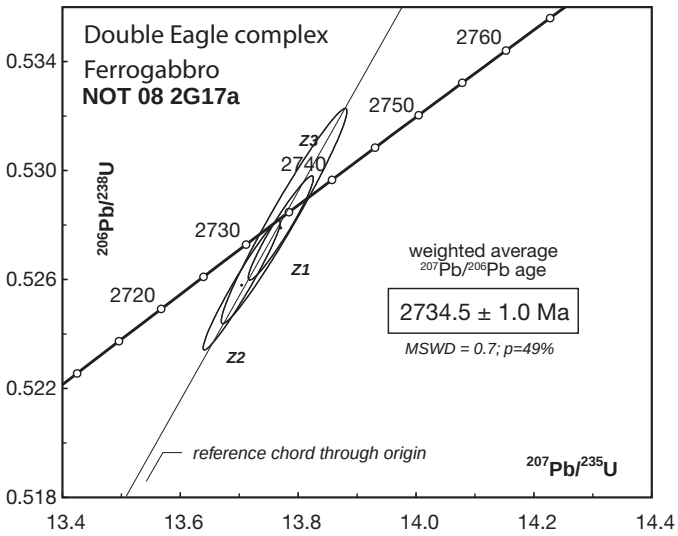

FIG. 5. Concordia diagram for sample NOT 08 2G17.

the McFaulds Lake VMS deposits. This, in turn, indicates that the Ring of Fire complex was probably emplaced within several kilometers of the surface, and that the volcanic suites above it were in some way related, if not actually comagmatic. The intrusion of the ultramafic rocks occurred at the approximate level of what is interpreted to be a major unconformity separating preexisting crystalline basement rocks that now occur within the Ring of Fire from the overlying volcanic and sedimentary sequence, which now is located outside the unconformity marked by the iron formation.

At the regional scale, the Ring of Fire complex was emplaced in an active volcanic belt on thinned lithosphere at the northern margin of the microcontinent now recognized as the North Caribou superterrane. This occurred ca. 2735 Ma, at least 15 m.y. prior to the eventual collision of the terrane with the North Superior superterrane ca. 2720 Ma. It is noteworthy that the Bird River complex of ultramafic and mafic intrusions, which also hosts Ni sulfide and chromitite deposits (Theyer et al., 1991), was intruded into the southern margin of the same microcontinent ca. 2745 ± 5Ma (Timmins et al., 1985), placing it well within the possible age span of a single plume-related large igneous province.

Geology of the Eagle's Nest Deposit

In general terms, the Eagle's Nest deposit is a subvertically dipping body of massive and net-textured magmatic sulfide minerals (i.e., pyrrhotite, pentlandite, chalcopyrite) and magnetite in the form of a sheet about 200 m long, as much as several tens of meters thick, and at least 1,000 m deep (Fig. 6). It strikes northeast-southwest and occupies the northwestern margin of a vertically inclined serpentinized peridotite dike, which is present in subcrop over a north-south strike length of about 500 m, with a maximum width of about 75 m. Near the surface, the massive sulfides are strictly confined to the northwestern tip of this intrusive body, and are bordered to the southeast by a thicker zone of net-textured sulfides, which are hosted by serpentinized peridotitic cumulates. At depth, there are occurrences of massive sulfides farther to the east within the dike, although they tend to be concentrated near

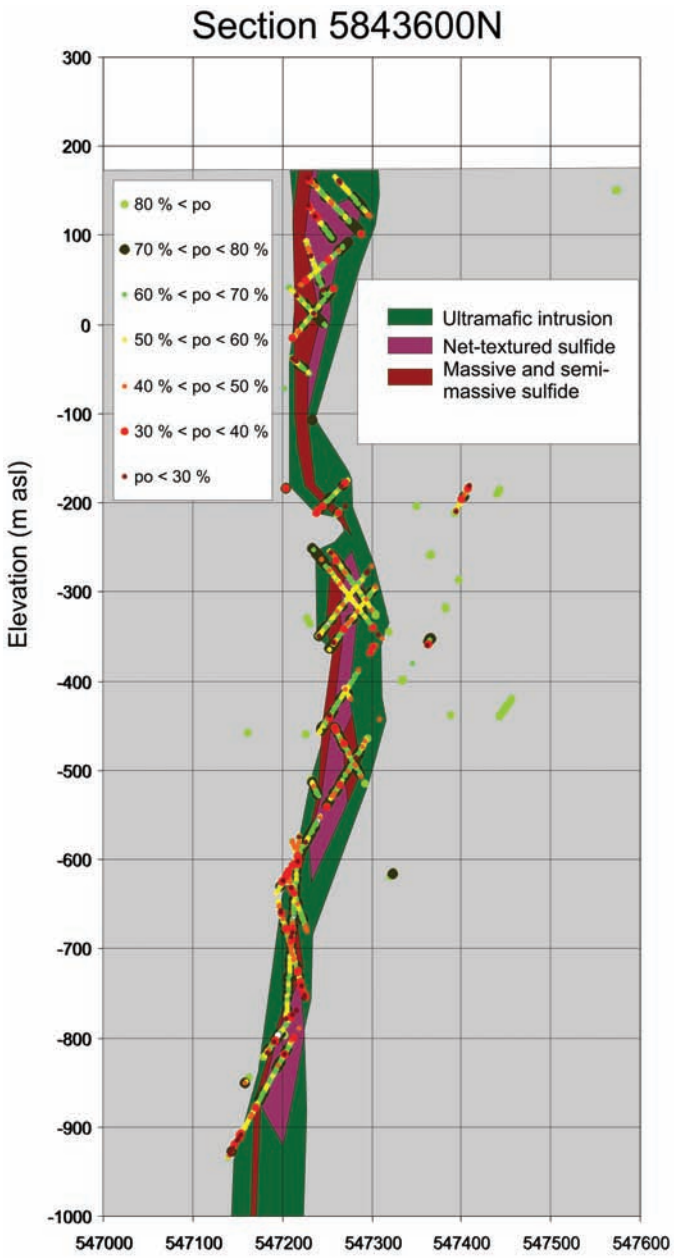

FIG. 6. Cross-sectional sketch of the Eagle's Nest deposit along east-west section 5843600N. The intrusion strikes north-south and extends about 200 m farther north than the section shown. It also extends about 300 m off section to the south. The granodiorite host rocks are shown in gray. Colored dots represent individual assays recalculated to 100 percent sulfide and colored according to normative pyrrhotite content. Samples with > 80 percent pyrrhotite are generally restricted to the host rocks and are not magmatic sulfides. Pyrrhotite contents in the range from 70 to 80 percent probably are mss cumulates, away from which all residual sulfide melt has drained. The remaining 20 to 30 percnet in these samples is generally all pentlandite, which was originally contained within the primary mss in solid solution. Samples in the range from 50 to 70 percent pyrrhotite are probably close to the original sulfide composition, whereas lower values are interpreted to be cumulate mixtures of iss and mss deposited from strongly fractionated residual sulfide liquids.

the western and northern extremities. The dike is closed off both at its northern and southern ends and plunges vertically or very steeply to the south. Although a considerable amount of local deformation is evident near the contacts, particularly

where they are occupied by massive sulfide, some intersections of the contacts have entirely escaped deformation and preserve chilled margins on both sides of the dike, indicating that the body is essentially still in place and not significantly deformed.

Rock types of the Eagle's Nest intrusion

There are several important facies in the intrusion which can be separated on the basis of texture and composition. The names presented here are based on recognizable cumulus crystal populations in these generally orthocumulate- to heteradcumulate-textured rocks. As discussed below, CIPW norm calculations show that prior to alteration, these rocks likely contained sufficient interstitial postcumulus plagioclase to place them within the field of melanocratic mafic equivalents of the rock types listed here (e.g., harzburgite might be reclassified as olivine melanorite).

Harzburgite: This rock contains about 75 percent submillimetric black serpentinized olivine primocrysts, many of which are enclosed by centimeter-scale, equant to euhedral oikocrysts of pyroxene, which are dominated by pale brown enstatitic orthopyroxene with lesser amounts of diopsidic clinopyroxene. Outside the oikocrysts, the matrix to the olivine crystals has been recrystallized to very fine grained ferromagnesian minerals, probably a mixture of chlorite and tremolite. There are also occasional centimetric oikocrysts of a deep reddish brown amphibole, which is interpreted to be relict postcumulus magmatic hornblende, in contrast to the abundant metamorphic tremolite-actinolite, which is also present. The texture suggests a heteradcumulate origin. The rock is cut by numerous subparallel veins along which millimeter-sized, equant magnetite crystals have grown either singly or as continuous chains.

Lherzolite: This rock comprises a dense granular aggregate of 1- to 3-mm grains of black serpentinized olivine and pale greenish-gray tremolite and chlorite pseudomorphs of pyroxenes. There is little intercumulus material and the rock appears to have been an adcumulate. Abundant magnetite, either dispersed throughout the rock or as veins, makes this peridotite highly magnetic.

The adcumulate peridotite grades into orthocumulate textures, wherein the primocrysts are surrounded by fine-grained recrystallized material of uncertain composition. The metamorphic growth of talc, serpentine, tremolite, and chlorite tends to obscure primary grain boundaries, with the result that orthocumulate rocks are generally difficult to classify according to their original modes. The only remnants of the original orthocumulate textures tend to be small domains where other phases, such as interstitial sulfide or oikocrysts of pyroxene, have preserved the forms of the primary olivine crystals. Some of the rocks classified as peridotite were probably olivine pyroxenites prior to metamorphism, but the distinction is generally impossible due to metamorphic destruction of primary phases.

Marginal gabbro: The orthocumulate-textured ultramafic rocks grade smoothly into a medium- to fine-grained mafic marginal facies that is gradational into the chilled margins described below. The mafic rocks are pale green and composed of fine, felted masses of tremolite-actinolite, chlorite, plagioclase, and zoisite or epidote. Alteration to a biotite-rich assemblage is common near the contacts, particularly in the mafic rock types. This biotite alteration transgresses contacts and produces rocks with ultrapotassic compositions and hence is considered to be metamorphic, rather than primary, in origin.

Much of the fine-grained mafic marginal rock contains abundant xenoliths of uncertain origin. The xenoliths are presently recognizable as ovoid patches with different color than their host, commonly rich in felsic minerals or magnetite, or both. Some of these inclusions consist of 50 to 100 percent magnetite, and in these cases we suspect that they are remnants of oxide-facies iron formation. Others contain sulfide minerals and may be fragments of sulfide-facies iron formation or sulfide-rich metasedimentary rock. In a few examples, the sulfide inclusions have sharp angular outlines and could conceivably be ripped-up fragments of sulfide iron formation that has not been melted in the cooled and highly contaminated magma. The inclusions generally show concentric layers resembling corona textures resulting from an incomplete process of reaction with the surrounding melt. In some cases these layers are very pronounced. The inclusion-rich gabbros generally also contain abundant ovoid 1- to 10-mm blebs of sulfide minerals.

Chilled margins: At the contact of the intrusion, the mafic marginal facies shows a gradual drop in grain size down to a mafic aphanitic chilled contact against the host rocks. This material resembles mafic dikes, and where such contacts are complicated by the presence of ductile shear zones, it may be impossible to be sure whether a sliver of fine-grained mafic rock is a remnant of the chilled margin of the intrusion or a part of a later mafic dike.

Mineralization

Massive sulfide mineralization: Massive sulfides at the Eagle's Nest deposit are made up of pyrrhotite, pentlandite, and chalcopyrite, with subsidiary accessory amounts of equant millimetric magnetite. All occurrences of massive sulfide have extremely high conductivity. In most examples these rocks are very coarse grained, with grain sizes as large as 1 cm in diameter and well-formed pentlandite porphyroblasts. Locally, pentlandite is aligned along microfractures, a texture that can only result from late- or postmetamorphic nucleation and growth. It is, therefore, important to recognize that even extreme ductile deformational textures which may have existed in the sulfide at peak conditions will have been overprinted by late recrystallization to coarse grain sizes.

There are many medium- to very fine grained massive sulfide breccia veins that are rich in silicate inclusions and may display pronounced gneissic foliation, which wraps around breccia clasts and are referred to as "durchbewegung" texture. These evidently highly deformed sulfide bodies have escaped annealing crystallization, indicating that the deformation continued well after cooling from the conditions at which heterogeneously nucleated pentlandite was formed.

In some cases, the massive sulfide texture grades into peridotite through a marginal zone in which silicate minerals are completely surrounded by sulfide minerals and are not in mutual grain contact. The margins of semimassive sulfide zones are ragged and irregular, with little resemblance to the tectonic admixtures described above as sulfide breccias.

Net-textured sulfide mineralization: In this texture, which is almost exclusively developed within the lherzolitic orthocumulates, the silicate minerals, mostly olivine, form a close-packed orthocumulate-textured framework, with interstices that are fully occupied by sulfide minerals. All examples of net-textured sulfides show very high conductivity and, hence, are easily detectable by the airborne geophysics. In a few examples at Eagle's Nest, net texture is occupied by large (as much as 10 cm), apparently primary, pyrrhotite oikocrysts, which completely fill the interstices of the peridotite orthocumulate texture.

Much of the net-textured sulfide mineralization at the Eagle's Nest deposit shows a distinct metamorphic fabric. Subparallel, millimeter-scale, wavy veinlets of sulfide minerals dominated by chalcopyrite are present throughout the rock, apparently the result of transfer of sulfide on the grain scale from the net texture into extensional features. This foliation is commonly best developed in moderately deformed parts of the deposit that also contain fine-grained sulfide breccias.

In the common "network" variant of net-texture, which occurs farthest from the massive sulfide bodies, the interstitial sulfide minerals are present along linear or sheet-like zones surrounded by barren orthocumulate-textured peridotite. The moderate to high conductivity of these zones confirms that the sulfide domains are well-connected in the third dimension, although they appear rather sparse on the face of the core.

Disseminated sulfide mineralization: Where sulfide modal abundance is well below 30 percent, the sulfides are found in small patches with cuspate terminations between silicate primocrysts. The largest of these cuspate domains may enclose several serpentinized olivine crystals, but they do not exceed 2 cm in total diameter and they remain completely separated from one another. Serpentinized peridotite containing disseminated mineralization has very low conductivity.

Cloud sulfide mineralization: Where metamorphic recrystallization of the silicate and sulfide minerals has been extreme, the primary separation of sulfide minerals into cuspate blebs between silicate primocrysts has been erased. This leaves a fine-grained rock consisting of randomly oriented hydrous silicate phases, with finely dispersed sulfide minerals occupying triangular patches between the silicate minerals, as well as within thin sheets along silicate mineral cleavage planes.

Country rocks and later intrusions

Granodiorite: Porphyritic granodiorite consists of millimeter- to centimeter-sized euhedral plagioclase and K-feldspar phenocrysts in a dark matrix of hornblende, mica, and quartz. Except for minor ductile shear zones and narrow granitic dikes, these felsic host rocks are very uniform at the deposit scale. Primary feldspars are mainly saussuritized and ferromagnesian minerals have been mostly replaced by secondary biotite, actinolite, and chlorite. A moderate tectonic foliation is locally defined by recrystallized ribbons of quartz in some places, but in others, a primary isotropic fabric is well preserved.

Recrystallized granodiorite: Along their contacts with the mafic-ultramafic intrusion, the felsic country rocks typically show a very distinct textural change over several centimeters, which is probably a contact metamorphic aureole. The resulting rock is almost aphanitic but contains a few relict phenocrysts of feldspar; texturally, these recrystallized granodiorites are rhyolitic. The ground mass is black or orange and may contain fractures surrounded by alteration haloes. Although these contacts are locally gradational into the adjoining mafic chilled margin over several centimeters, they are commonly quite sharp.

There are several dikes of aphanitic felsic rock within the peridotite. These dikes closely resemble the aphanitic thermal contact aureole caused by the ultramafic intrusion in the granodiorites. They are surrounded by light green pyroxenite alteration zones in the peridotite.

Mafic dikes: There are several narrow, dike-like intrusions of material that closely resemble the finer-grained marginal facies of the main mineralized intrusion. They are locally gradational into ultramafic cores similar to the orthocumulate-textured rocks of the main Eagle's Nest intrusion. The dikes have undergone similar amounts of ductile deformation and have the same mineralogical composition and texture as the gabbroic marginal facies of the Eagle's Nest intrusion, and hence are considered to be members of the same intrusive suite. At least one of these minor intrusions is also weakly mineralized with blebs of sulfide minerals in a xenolith-rich gabbro facies, although the relationship of the sulfides to the main mineralized bodies is uncertain.

Brown micaceous dikes: Several very fine grained, brown micaceous dikes are present both within and outside the main intrusion. They are commonly present as the matrix to igneous breccias, made up of mixed clast populations of granodiorite and ultramafic rock, some of which are evidently preexisting net-textured parts of the mineral deposit. They locally show extreme bimetasomatic reaction zones against the ultramafic cumulate rocks, as well as against granodiorite, and are commonly back-veined by sulfides where they cross mineralization. In rare instances, relict portions of the interiors of these fine-grained dikes lack the potassic and nearly ubiquitous brown micaceous alteration.

Gray porphyritic mafic dikes: These fine-grained dikes are sparsely porphyritic, with needle-shaped soft black pseudomorphs after some ferromagnesian mineral. They form net-veined complexes along with the brown micaceous dikes in the granodiorite, especially along the eastern and southern margins of the main Eagle's Nest dike. There is a complete continuum in color and composition between the gray porphyritic dikes and the brown micaceous dikes.

Structure of the mineralized intrusion

Based on the examination of core from more than 70 diamond drill holes, we have established a working model of the form and genesis of the Eagle's Nest intrusion. The contact relations and the distribution of the lithofacies described above are critical to understanding the origin and disposition of the deposit. The Eagle's Nest intrusion contains a large proportion of olivine cumulates that are not representative of a liquid composition, but it lacks any large complementary body of mafic residue from which these cumulates might have been extracted. Furthermore, the intrusion contains far more sulfide than could have formed from the amount of

silicate rock presently enclosed within its contacts (cf. Barnes, 2007). We, therefore, conclude that the intrusion is a conduit through which a large volume of mafic or ultramafic magma has passed and into which olivine and sulfide liquid were accumulated from the through-going magma.

The intrusive rocks show a gradual zonation at the eastern margin of the intrusion from peridotite, through the medium-grained gabbroic facies, and to a fine-grained chilled margin against the enclosing granodiorite. Along the southern portion of the eastern contact, intrusive breccias have been observed, wherein brown micaceous dikes and gray porphyritic mafic dikes form the matrix enclosing stoped angular clasts of granodiorite and transported clasts of barren or weakly mineralized peridotite. Structures range from obvious net-veins in which breccia clasts remain in situ, to clearly transported textures in which all clasts are rounded and include exotic rock types.

The western margin shows more complicated contact relations. Some intersections through this contact have preserved chilled margins along which the blebby xenolith-rich marginal facies of the intrusion is chilled against recrystallized aphanitic granodiorite. The chilled margins clearly show that the contact is fundamentally an intrusive contact. However, most intersections of the western contact contain abundant evidence of ductile deformation, including ductile shear zones in the mafic rocks, extensive fabric development in the net-textured sulfide, and the nearly ubiquitous development of sulfide breccias, either directly in the contact with the host rocks or within the intrusion close to the contact. The western margin is, therefore, most likely an in-place, tectonically modified intrusive contact.

The most northerly drill holes intersected several isolated mafic to ultramafic dikes, at least one of which is composed of the blebby xenolith-rich marginal facies of the main intrusion. The mafic dikes are, therefore, interpreted as marginal apophyses of the main intrusion.

The main mineralized intrusion, as defined by its eastern and western chilled margins, is internally differentiated into several distinct zones definable by variations in sulfide mineral textures. In general, the massive sulfides are located adjacent to the chilled western margin and are succeeded to the east by the net-textured sulfides. Between the net-textured peridotite-hosted mineralization and eastern margin of the intrusion, there is weakly mineralized or barren ultramafic and mafic rock. Much of the weakly mineralized peridotite immediately east of the net-textured mineralization displays the network texture defined above.

In the context of models of sulfide migration through crystal mushes (e.g., Chung and Mungall, 2009), we can use the distribution of sulfide mineralization styles to infer the original orientation of the intrusion. The boundary between the net-textured sulfide domain and the barren ultramafic orthocumulates may be considered an approximation to a paleohorizontal surface, because the net-textured sulfide would have migrated laterally to form a relatively level surface within the crystal mush after reaching an impermeable layer or contact zone near the bottom of the mush. The inferred paleohorizontal surface strikes approximately 30° in all level plans, and has a vertical dip. At the time of emplacement, the Eagle's Nest intrusion was shaped like a sword blade, with a horizontal long axis striking due south and an intermediate axis dipping about 30° to the east. Sulfide liquid collected within the olivine crystal mush at the base of this dike, creating a keel of net-textured sulfide along the bottom, with pods of massive sulfide near the lower contact.

The margins of the massive pods are typically ragged and irregular, apparently preserving the textures at the point where sulfide liquid had completely displaced the olivine crystal mush. The observation that the massive sulfide is present as pods and irregular bodies within the lower portion of the net-textured domain is not consistent with a scenario in which olivine crystals were pushed down into a preexisting pool of sulfide liquid. Rather, we suggest that continued accumulation of sulfide melt into an olivine crystal mush proceeded first by expelling interstitial silicate melt (e.g., Chung and Mungall, 2009) and then by inflating bodies of pure sulfide liquid within the semi-rigid framework of olivine crystals. Network-textured sulfides formed within the olivine crystal mush immediately above the net-textured zone, and served as pathways for the downward percolation of sulfide melt into the crystal mush from a through-going mass of sulfide-saturated magma near the top of the conduit. Disseminated patches of sulfide represent isolated droplets that were prevented from downward migration by capillary forces, causing them to remain stranded within the crystal mush above the net-textured zone.

The common occurrence of aphanitic-textured (i.e., rhyolitic) metamorphic aureoles in the granodiorite country rocks, coupled with the observations of rhyolitic dikes mantled by orthopyroxenite reaction zones within the peridotite of the Eagle's Nest intrusion, suggests that the wall rocks were commonly heated above their melting points. After the cumulate rocks of the intrusion had become partially solidified, they underwent brittle fracturing, allowing the host-rock melts to form veins crossing the ultramafic intrusion itself (i.e., back-veining), while it was still hot enough to react with these silica-rich melts and form a pyroxenite halo.

Subsequent tectonic activity rotated the Eagle's Nest body about 90° downward to the south around a horizontal rotational axis striking east-west. The result is that the formerly horizontal surface bounding the net-textured sulfide domain now dips vertically and strikes to the northeast. The former top of the dike is now represented by its southeastern extremity, whereas its former base now sits at the northwestern tip where the massive sulfide bodies are located.

Consanguineous igneous breccias within the intrusion, particularly along its southeastern margin, are indicative of synmagmatic brittle faulting. We suggest that this, combined with the inferred shallowly dipping form of the dike at the time of emplacement, is consistent with intrusion of the dike into a normal fault. This, in turn, is suggestive of extensional tectonics contemporaneous with the formation of the Ring of Fire complex. Recognition of other such normal faults in the basement to the Ring of Fire iron formation might help in the recognition of other prospective intrusive environments.

The presence of orthocumulate textures in the ultramafic rocks is an indication that the intrusion was cooled fairly rapidly, before annealing recrystallization and compaction could eliminate intercumulus liquid. Orthocumulate textures in the dike are in sharp contrast to the ubiquitous adcumulate

textures that are prominently displayed by the thicker, sill-like intrusions that host the Blackbird chromitite deposit immediately to the south and east of the Eagle's Nest dike.

Several other ultramafic dikes, some containing magmatic sulfide mineralization, exist within 15 km of the Eagle's Nest dike. The most notable of these is the AT12 occurrence (Fig. 3), which shows rock types, textures, and sulfide compositions identical to Eagle's Nest, but has not yet been found to contain significant tonnages of sulfide mineralization. Like the Eagle's Nest dike, the AT12 dike is separate from, but directly northwest of a much larger sill-like accumulation of adcumulate-textured ultramafic rocks that include thick accumulations of chromitite. Eagle's Nest, AT12, and several other apparently cogenetic peridotite dikes all show similar structural relations with the enclosing granodiorite and the other intrusions of the Ring of Fire complex.

Lithogeochemistry

Analytical methods

Several hundred samples of drill core from the Eagle's Nest deposit and related intrusions and country rocks have been collected for lithogeochemistry. Analyses were done at Activation Laboratories Ltd of Ancaster, Ontario. Samples were crushed with a steel jawcrusher and pulverized in a puck mill, after which a 1-g sample was fused in a lithium metaborate-tetraborate flux in an induction furnace. The fused sample was poured into 5 percent nitric acid while still molten and mixed until dissolved. Major and trace element concentrations were determined by inductively coupled plasma (ICP) spectrometry of the solutions.

The compositions of mineral grains in several polished thin sections were determined by electron probe microanalysis (EPMA). The instrument used is a Cameca SX50 equipped with three tunable wavelength-dispersive X-ray spectrometers, employed with 20 kV accelerating voltage, and a 30 nA beam current focused on a 1-μm spot. Peaks were counted for 20 s for major elements and 40 s for minor constituents, and background counting of the same total duration was performed on both sides of each peak with a linear correction. The matrix correction method was ZAF or Phi-Rho-Z (e.g., Armstrong, 1988) using mass absorption coefficients from the CITZMU dataset (Henke and Ebisu, 1974). Oxygen was calculated by matrix stoichiometry and included in the matrix correction. Synthetic and natural mineral standards were used to calibrate the instrument, and standard intensities were checked routinely to correct for drift through time.

The compositions of representative rock samples recalculated on an anhydrous basis are presented in Table 1. Also shown are the average compositions of olivine, orthopyroxene, and spinel grains from one thin section of olivine melanorite taken from an unusually fresh sample (NOT-07-17-33).

Major element geochemistry

The most magnesian of the samples that can be recognized unequivocally on textural grounds as part of the chilled margins and thus representative of solidified liquid compositions (NOT-08-2G12-73.6) contains 18.56 percent MgO (Fig. 7). Taking the division between picritic basalt and komatiite to fall at 18 wt percent MgO (e.g., Arndt, 2003), this liquid would be considered to be a komatiite. The high concentrations of incompatible lithophile elements for this sample are strongly suggestive of contamination by crustal rocks. This indicates that the parental liquid for this suite most likely had MgO contents well within the range of komatiitic magmas, which are well known to host Ni sulfide deposits (e.g., Lesher and Keays, 2002).

The variation of total iron expressed as FeO* against MgO, both anhydrous, in the Eagle's Nest and related rocks is shown in Figure 7. The AT12 ultramafic dike compositions are included because they are considered to be comagmatic with the Eagle's Nest dike, but have undergone much less potassic alteration and are considered to be more representative of genuine liquid compositions. One relatively fresh sample (NOT-07-17-33) was chosen to represent the bulk of the ultramafic rock within the dike, because it presents numerous examples of olivine and pyroxene grains that have not been altered to hydrous minerals. The transition from the ultramafic core of the dike to its gabbroic marginal facies and fine-grained chilled margin is evidently accompanied by a rapid decrease in MgO content.

Trace element geochemistry

The abundances of trace elements in several samples are shown normalized to primitive mantle (McDonough and Sun, 1995) in Figure 8. The highest incompatible element abundances are shown by the granodiorite, whereas the orthocumulate-textured ultramafic rocks show the lowest values. All samples show a distinct upward slope to the left, mirroring the large-ion lithophile element (LILE) enrichment that is typical of Archean granitoids (e.g., Gao et al., 1998). A prominent negative Nb anomaly is present in the granodiorite, in accordance with its probable origin as an arc magma. Samples of the chilled margin of the AT12 and Eagle's Nest ultramafic dikes share the LILE-rich and relatively Nb-depleted characteristics of the host granodiorite. The two examples of chilled margin samples from the Eagle's Nest are taken just 10 cm apart; the higher LILE enrichment is shown by the sample directly adjoining the granodiorite host, whereas the less-enriched sample is from 10 cm inside the contact. On the other hand, in the most olivine-rich sample shown (NOT-07-17-33), the Nb anomaly is effectively absent and the rare-earth elements (REE) show only a slight increase from heavy REE to light REE; only U is highly enriched in this sample.

Lithogeochemical interpretations

The controls on the compositions of liquids in the Eagle's Nest and AT12 intrusions are likely to have included crystal sorting, and contamination by melting or dissolution of wall rocks. Simple modeling allows for better understanding of the relationships between different rocks in this suite. Working on the hypothesis that the parental liquid of the ultramafic intrusion might have been extracted from the depleted upper mantle, as is typical of Neoarchean komatiites (e.g., Herzberg and O'Hara, 1998; Arndt, 2003), we attempted to model a high-MgO liquid composition by removing small amounts of granodiorite from the most magnesian chilled margin composition in our suite. This was achieved by assuming that the concentration of an element in the contaminated liquid C_{cont}

Table 1. U-Pb Isotope Data for Zircons from the Double Eagle Complex, Ontario

Sample fraction	Analysis no.	Description	Wt (μg)	U (ppm)	Th/U	Pb* (pg)	Pb_C (pg)	$^{206}Pb/^{204}Pb$	$^{206}Pb/^{238}U$	± 2σ	$^{207}Pb/^{235}U$	± 2σ	$^{207}Pb/^{206}Pb$	± 2σ	Age (Ma) $^{206}Pb/^{238}U$	± 2σ	Age (Ma) $^{207}Pb/^{235}U$	± 2σ	Age (Ma) $^{207}Pb/^{206}Pb$	± 2σ	Disc. (%)	Corr. Coeff.
NOT07-06		Tonalitic host																				
Z1	MAH8179	1 cls, clr, shrt flat prism	3.1	104.6	0.354	185.6	0.27	39244	0.532964	0.001099	14.22753	0.03403	0.193611	0.000179	2753.9	4.6	2765.0	2.3	2773.1	1.5	0.8	0.924
Z2	MAH8180	1 cls, clr, 2:1 prism	1.1	83.7	0.369	49.9	0.65	4471	0.535899	0.001214	14.31118	0.03897	0.193683	0.000190	2766.3	5.1	2770.6	2.6	2773.7	1.6	0.3	0.939
Z3	MAH9008	1 cls, clr, prism tip	1.0	88.9	0.386	53.4	0.30	10387	0.537461	0.001246	14.35021	0.03816	0.193646	0.000173	2772.8	5.2	2773.1	2.5	2773.4	1.5	0.0	0.945
NOT08-2G-17		Ferrogabbro																				
Z1	MAH9199	1 cls, clr, crk eq frag	1.2	52.5	0.835	33.8	0.39	4601	0.527865	0.001564	13.77018	0.04568	0.189198	0.000190	2732.5	6.6	2734.0	3.1	2735.2	1.7	0.1	0.955
Z2	MAH9200	1 cls, clr, crk eq frag	0.5	66.1	0.887	21.4	0.16	7129	0.525756	0.001943	13.70368	0.05373	0.189039	0.000185	2723.5	8.2	2729.4	3.7	2733.8	1.6	0.5	0.969
Z3	MAH9201b	1 cls, clr, crk eq frag	0.5	36.3	1.004	12.1	0.24	2529	0.528303	0.003229	13.77528	0.08758	0.189111	0.000276	2734.3	13.6	2734.4	6.0	2734.4	2.4	0.0	0.973

Notes: All analyzed fractions represent least magnetic, chemically abraded single zircon grains, free of inclusions, cores or cracks, unless otherwise noted

Abbreviations: clr = clear, cls = colorless, el = elongate, irr = irregular, eq = equant, frag - fragment,crk = contains crack

Wt = weight (micrograms). Pb* is total amount (in picograms) of radiogenic Pb. Pb_C is total measured common Pb (in picograms) assuming the isotopic composition of laboratory blank: 206/204 - 18.221; 207/204 - 15.612; 208/204 - 39.360 (errors of 2%)

Pb/U atomic ratios are corrected for spike, fractionation, blank, and, where necessary, initial common Pb; $^{206}Pb/^{204}Pb$ is corrected for spike and fractionation

Th/U is model value calculated from radiogenic $^{208}Pb/^{206}Pb$ ratio and $^{207}Pb/^{206}Pb$ age assuming concordance. Disc. (%) - percent discordance for the given $^{207}Pb/^{206}Pb$ age

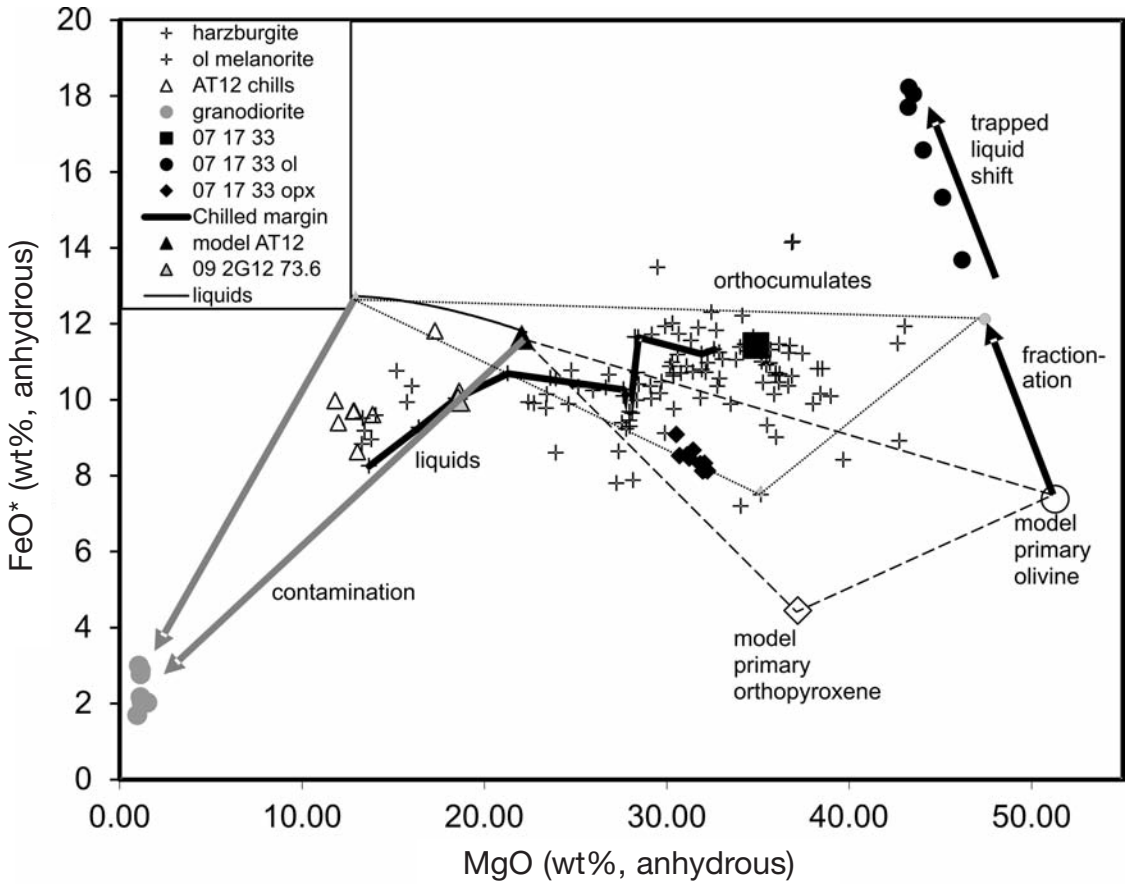

FIG. 7. Total FeO versus MgO for whole rocks and minerals from the Eagle's Nest deposit. Chilled margin compositions from the AT12 dike and model compositions are shown for comparison. Open triangles show the compositions of chilled margin samples from the AT12 dike of which NOT-08-2G12-73.6 (gray shaded triangle) is the most primitive. Crosses shown samples from Eagle's Nest that are not obviously altered, including gabbroic or chilled margin samples toward the left of the diagram and olivine melanorite or harzburgite cumulates toward the right. A solid black line connects samples that were taken along a single length of drill core NOT-08-36 from 226 to the chilled margin at 256.7 m (both samples are listed in Table 1). The composition of the model parental liquid is shown as a large solid black triangle. Emerging from this point is a trend of model liquid compositions calculated as described in the text. The composition of the first olivine that would have formed from the model parent magma is shown as a large open circle. Also shown is the composition of postcumulus orthopyroxene that might grow at equilibrium from the same liquid, assuming a K_D of 0.23 (Roeder and Emslie, 1970), along with tie-lines connecting the liquid and the two possible solid phases. An arrow is shown passing from the model parental melt through the actual chilled margin sample from which it was sampled toward the granodiorite host rocks, and another similar arrow passes through more evolved compositions; between these two arrows lie all of the putative liquid compositions represented by chilled margins of the Eagle's Nest and AT12 dikes.

could be modeled as a linear mixture of a model granodiorite contaminant C_{gran} and a primitive melt with C_{prim} as shown:

$$C_{cont} = XC_{gran} + (X-1)C_{prim},$$

where X is the weight fraction of granodiorite and (1-X) is the weight fraction of primitive melt in the mixture. Rearranging,

$$C_{prim} = \frac{C_{cont} - XC_{gran}}{X-1}.$$

We used a granodiorite composition based on sample NOT-07-10-78.5. However, because the estimated value of C_{prim} is highly sensitive and becomes negative when an excessive amount of granodiorite is added to the model mixture, we were forced to make slight changes in the granodiorite composition to achieve a match to all of the lithophile elements simultaneously. The difference between this composition and the actual granodiorite is insignificant (Fig. 8). The resulting primitive liquid composition is a mixture of 83 percent of this liquid with 17 percent of the model granodiorite (Fig. 8), which would produce a liquid with the exact composition of the chilled margin at AT12. The model compositions are shown in Table 1.

This simple modeling demonstrates it is plausible that a primitive magma with a slightly depleted LILE signature was parental to the intrusive suite, and that it acquired its LILE-enriched composition through assimilation of the country rocks. The ubiquitous presence of partially melted granodiorite lining the contacts, and dikes of granodioritic material back-veining the ultramafic intrusion, would tend to support this view. Local contamination is also consistent with the

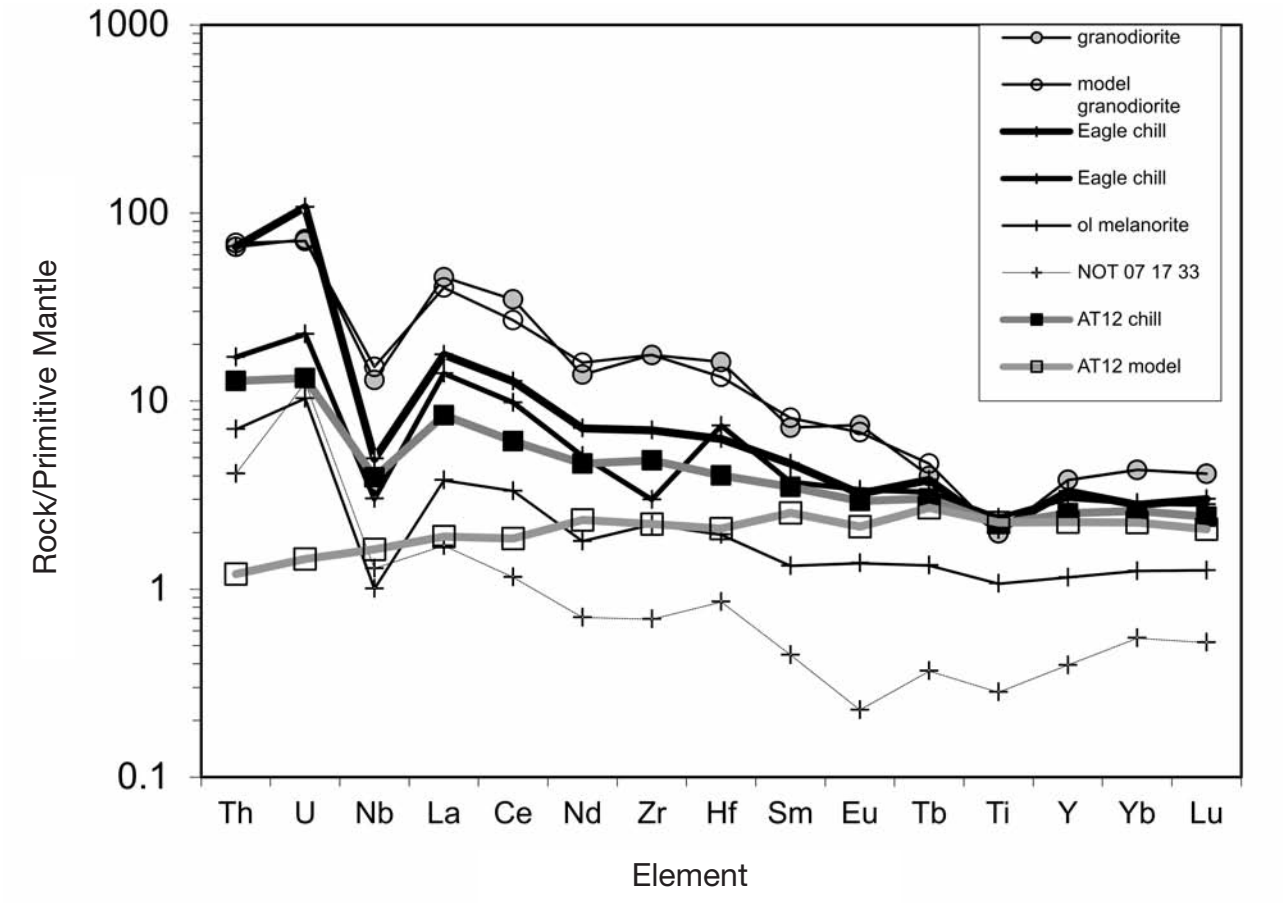

FIG. 8. Trace element ratio plot comparing cumulate rocks, chilled margins, and host rocks from the Eagle's Nest deposit and AT12 occurrence along with model compositions. The model granodiorite used in the estimation of degree of contamination is shown with open circles, compared with the actual host rock composition shown with closed circles. The resulting model parental liquid composition is shown with open square symbols.

extreme enrichment in LILE observed over the last few centimeters approaching the contact in drill hole NOT-08-36, an enrichment that is not matched by corresponding changes in Fe/Mg ratio and hence cannot have resulted from crystal sorting.

The compositions of liquids derived from this putative parental liquid were calculated by estimating the composition of olivine that would coexist with it at equilibrium using a Mg/Fe K_D of 0.3 (Roeder and Emslie, 1970), removing a small aliquot of this olivine from the liquid, and repeating on the resulting modified liquid composition. The compositions of olivine and orthopyroxene that would coexist with a derivative magma resulting from olivine removal down to an MgO content of 13 percent are also shown; these are quite close to the more magnesian compositions actually observed in the intrusion, as exemplified by sample NOT 07 17 33. The progression from these values to increasing FeO and diminishing MgO in the actual olivine and orthopyroxene compositions can be attributed to a trapped liquid shift (e.g., Barnes, 1986; Cawthorn et al., 1992), as the primocryst compositions continuously reacted with interstitial melt during cooling. The slight offset of actual pyroxene compositions to lower FeO and MgO is due to the presence of minor other components in solid solution, such as diopside, Ca-Tschermaks, and minor TiO_2 and Cr_2O_3. Because the orthopyroxene in these rocks was predominantly postcumulus in origin, the original rocks can be considered to a first approximation to have been mixtures of primary olivine and interstitial liquid. Applying the lever rule, one can see qualitatively that the rocks identified in Figure 7 as orthocumulates are probably composed of approximately 40 to 60 percent olivine with complementary amounts of interstitial liquid. The trend to lower MgO in the gabbroic marginal facies can be interpreted as a result of the presence of decreasing amounts of olivine in the rocks. The scatter in the ultramafic rock compositions probably results from variable amounts of compaction and postcumulus growth of pyroxene.

We conclude that the liquids captured as chilled margins in these two intrusions owe their compositional diversity to a combination of fractional crystallization of olivine and varying degrees of assimilation of their granodioritic host rocks.

Sulfide chemistry

The compositions of Ni and Cu-bearing sulfide minerals are recalculated to nominal 100 percent sulfides (Fig. 9). This calculation was done by assuming that all Ni is hosted by pentlandite containing equal weight fractions of Ni and Fe, that all Cu is hosted by chalcopyrite, and that all S not

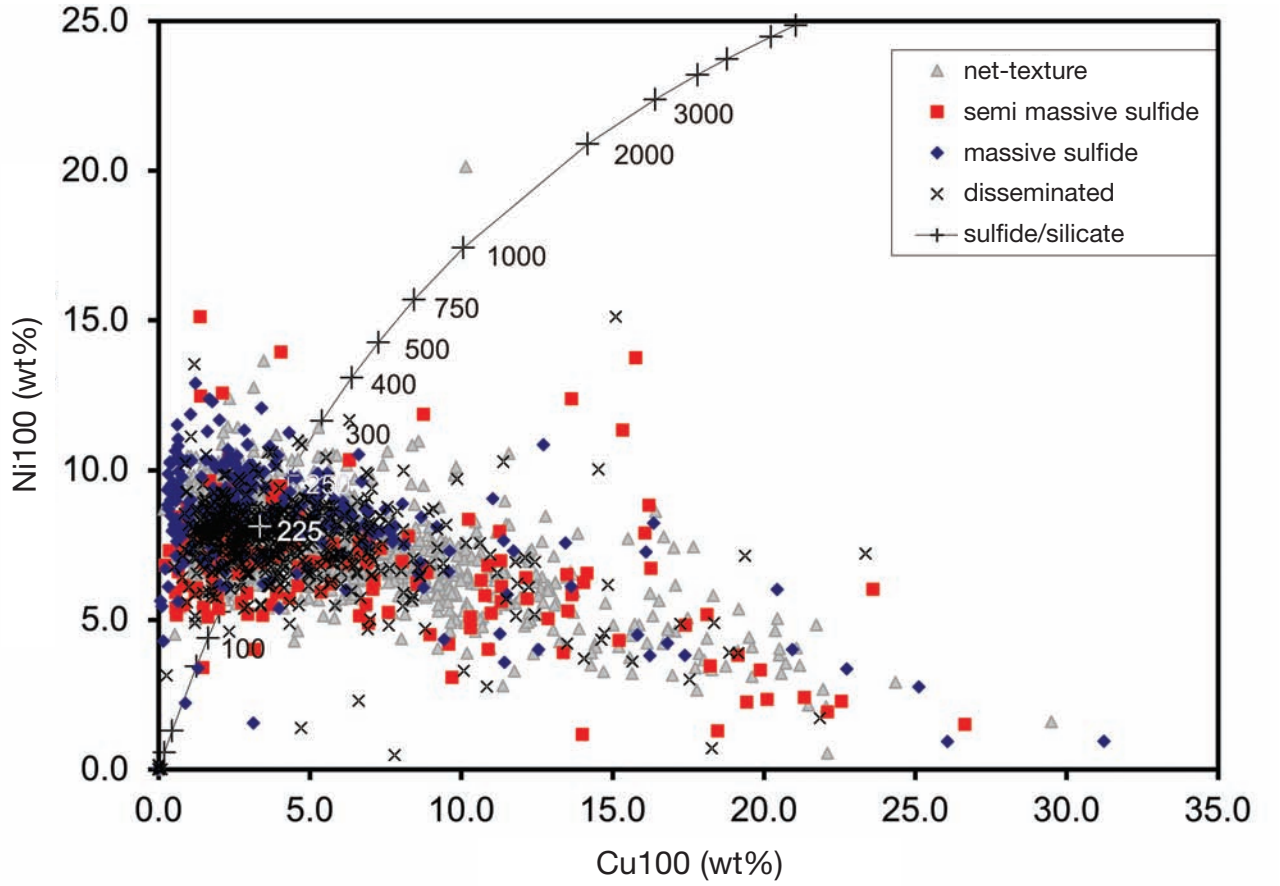

FIG. 9. Variation of Ni100 versus Cu100 for mineralized samples from the Eagle's Nest deposit. The data are classified such that samples containing between 2.5 and 5.5 percent S are considered to contain disseminated sulfides or minor quantities of narrow vein sulfides, between 5.5 and 12 percent S are net-textured sulfides, between 12 and 25 percent S are semimassive sulfides, and above 25 percent are massive sulfides, which most typically contain about 34 percent S. Also shown is the trend followed by the model sulfide liquids in equilibrium with the putative parental silicate magma (Campbell and Naldrett, 1979).

required to compose pentlandite and chalcopyrite is in pyrrhotite. Owing to the presence of small amounts of Ni in solid solution in silicate minerals, probably mostly in serpentine, this calculation produces spuriously high Ni100 values in sulfur-poor rocks. Accordingly, we have restricted our data set in Figure 9 to samples containing more than 2.5 wt percent S.

Interpretation of sulfide chemistry

The origins of the sulfides are slightly enigmatic. It is generally accepted that to form a mass of immiscible sulfide liquid on the scale observed at the Eagle's Nest deposit, a mafic or ultramafic magma must become contaminated by crustal rock and in most, but not all, cases the assimilation of crustal S is also considered necessary (e.g., Naldrett, 2004; Mungall 2005; Seat et al., 2007, 2009). However, at its present level of exposure, the mineralized intrusion is entirely surrounded by sulfur-poor felsic intrusive rocks. We suggest that the presence of abundant magnetite-rich xenoliths in the intrusion records assimilation of iron formation, which may have added sufficient sulfide to the magma to induce sulfide liquid saturation. The conduit has carried the slurry of sulfide droplets and small xenoliths to their current location. This in turn suggests that the Eagle's Nest deposit resides in a large magmatic system with lateral extents at least as great as the distance to the nearest iron formation. Iron formations are not uncommon in the older polydeformed supracrustal sequence within the Ring of Fire dome, and they are certainly abundant along the unconformity below which the Eagle's Nest dike was intruded.

The data in Figure 9 are distributed along a prominent trend from Cu-poor and Ni-rich to Ni-poor and Cu-rich. This type of trend has been argued to result from dispersion of the sulfide compositions along a mixing line between early-formed monosulfide solid solution (mss) and later cumulus intermediate solid solution (iss) (Mungall, 2007a). Upon cooling, the mss exsolves into coexisting pentlandite and pyrrhotite, whereas the iss may either exsolve cubanite and chalcopyrite or equilibrate with surrounding Fe-rich sulfides and silicates to form chalcopyrite plus pyrrhotite. Small volumes of former sulfide melt, rich in both Ni and Cu, will be somewhere in the system, perhaps partly represented by a few outliers which are present well above the trend. It is also possible that if such fractionated sulfide melts existed, they may have drained out of the main dike and could, therefore, be found to the north of the currently recognized orebody.

The compositions of massive and net-textured sulfides generally overlap, indicating that whatever processes allowed the differentiation of the sulfide melt operated equally on both. Because massive and net-textured ores are very well-interconnected reservoirs of melt when they form, this is not surprising. It is somewhat more surprising that the samples in the semi-massive category show a distinctly lower average Ni content than either the massive or the net-textured samples. The reason for this difference is unclear.

The disseminated sulfides are much more tightly clustered in composition than are any of the other sulfide classes. In the context of the models proposed by Chung and Mungall (2009), the tight compositional clustering would suggest that the disseminated sulfides are trapped aliquots of sulfide melt. They became isolated in pores among the silicate minerals of the orthocumulate-textured ultramafic rocks and were subsequently unable to interact with other sulfide grains and masses. These compositions, therefore, probably record the original composition of the sulfide melt that was accumulating in the dike.

Initial modeling attempts failed to produce trends that could simultaneously agree with the Ni-Cu and PGE concentrations of the silicate magma and the sulfide ore. Nickel concentration in the modeled sulfide liquids was consistently much higher than actually measured. This is an indication that the magma crystallized some olivine prior to reaching sulfide saturation, as is expected for sulfide-undersaturated ultramafic magmas when they first encounter country rocks and begin to evolve by contamination and concomitant olivine crystallization (e.g., Mungall, 2007b). The effects of removal of 10 wt percent olivine from the model parental magma were estimated by removing Ni from the melt in the olivine fractionation process (Fig. 7), using a K_D for Ni in olivine from Hart and Davis (1978). Although Li et al. (2003) have shown that the partitioning of Ni depends, in part, on the sulfur content of a magma, because the Eagle's Nest system was active at much higher temperatures, and consequently lower K_D than would apply to MORB compositions, the Hart and Davis (1978) values were assumed to be more applicable here. At the same time, it was assumed that Cu and Pt would behave as incompatible elements, leading to their slight enrichment in the olivine-depleted magma. Partition coefficients were taken from Mungall (2005).

Using mass balance constraints, the best match for the compositions of the disseminated sulfide samples is achieved at a silicate/sulfide mass ratio (i.e., the '*R*' factor of Campbell and Naldrett, 1979) of 225. This implies that there was an excess of approximately 0.44 wt percent of sulfide liquid present in the magma, an amount more than four times the typical solubility of sulfide in mafic magmas (e.g., Mavrogenes and O'Neill, 1999). To produce this silicate/sulfide ratio in a system closed to S, by some combination of assimilation and fractional crystallization from a magma initially containing about 0.1 percent S, would require the solidification of more than 80 percent of the amount of silicate liquid initially present. This is not consistent with the mafic and ultramafic nature of the rocks hosting the mineralization. The estimated amount of excess S supports the need for some assimilation of crustal sulfur to generate the significant volumes of magmatic sulfide. If the assimilant that introduced the sulfur was a typical sulfide-rich metasedimentary rock with about 10 modal percent sulfide minerals, then this amount of sulfur would represent the addition of about 4.4 wt percent of contaminating host rock to the magma. If the contaminants were somewhat less sulfide rich than 10 modal percent, then the amount of contamination could easily approach the 13 wt percent of crustal material implied by the modeling (e.g., Figs. 7, 8). Although the models assume the granodiorite to be the contaminant, one might expect generic clastic metasedimentary rocks on the flanks of an Archean protocontinent, including minor interbedded banded iron formation as the source of sulfur, to have compositions rather similar to granodiorite, and hence the two sets of model results are compatible with each other.

The variation of Pt100 with Cu100 (Fig. 10) shows the match between model and disseminated sulfide is reasonably good at $R = 225$. However, there are aspects of the relationship that cannot easily be explained by purely magmatic processes. Although the net-textured and disseminated sulfides generally fall in a fairly restricted range of Pt100, the dispersion of Pt tenor to extremely low values in the massive sulfide falls far below any plausible range attainable by fractional or equilibrium crystallization of mss. Consequently, this depletion in Pt100 must have been caused by metamorphic or late magmatic fluid redistribution, and the considerable mass deficit of Pt represented by the Pt-depleted massive sulfides must be matched by a complementary reservoir somewhere in the deposit that is highly enriched in Pt. There are a few occurrences in the Eagle's Nest deposit where Pt grade reaches several hundred ppm over true widths on the order of 1 m, particularly in association with deformation zones lined by sulfide breccias extending into the granodioritic country rocks. One such vein system is exemplified by concentrations of 389 ppm and 1597 ppm Pt100 (Fig. 10). These are samples of massive sulfide containing abundant visible sperrylite, with true Pt grades prior to recalculation to nominal 100 percent sulfides are 351 ppm over 50 cm and 1170 ppm over 15 cm. Considering the dynamic range of Pt concentrations (Fig. 10), it is worth bearing in mind that one m^3 of massive sulfide containing 351 ppm Pt could contain all the Pt formerly contained in 100 m^3 of massive sulfides formerly containing 3 ppm Pt, but which now are Pt-depleted. It is easy to overlook the significance of a small number of PGE-rich assays, considering them as mere outliers, when in fact they may represent a small reservoir into which much of the PGE budget of the entire intrusion has been sequestered.

It is interesting to consider the spatial variation of metal tenor within the deposit. The norm calculation used to determine nominal 100 percent sulfide compositions also estimates nominal modal abundances of pyrrhotite. Since, in this context, any sulfide mineral that is not pyrrhotite is an ore mineral, the normative abundance of pyrrhotite is inversely correlated to the tenor and, therefore, the value of the mineralization. There is also a correspondence between high normative pyrrhotite abundance and the original presence of high abundance of cumulus mss compared to the amount of ore metal-rich residual sulfide liquid. We have, therefore, mapped the distribution of normative pyrrhotite onto the schematic geological cross section in Figure 6 to see where the cumulate-rich parts of the deposit are.

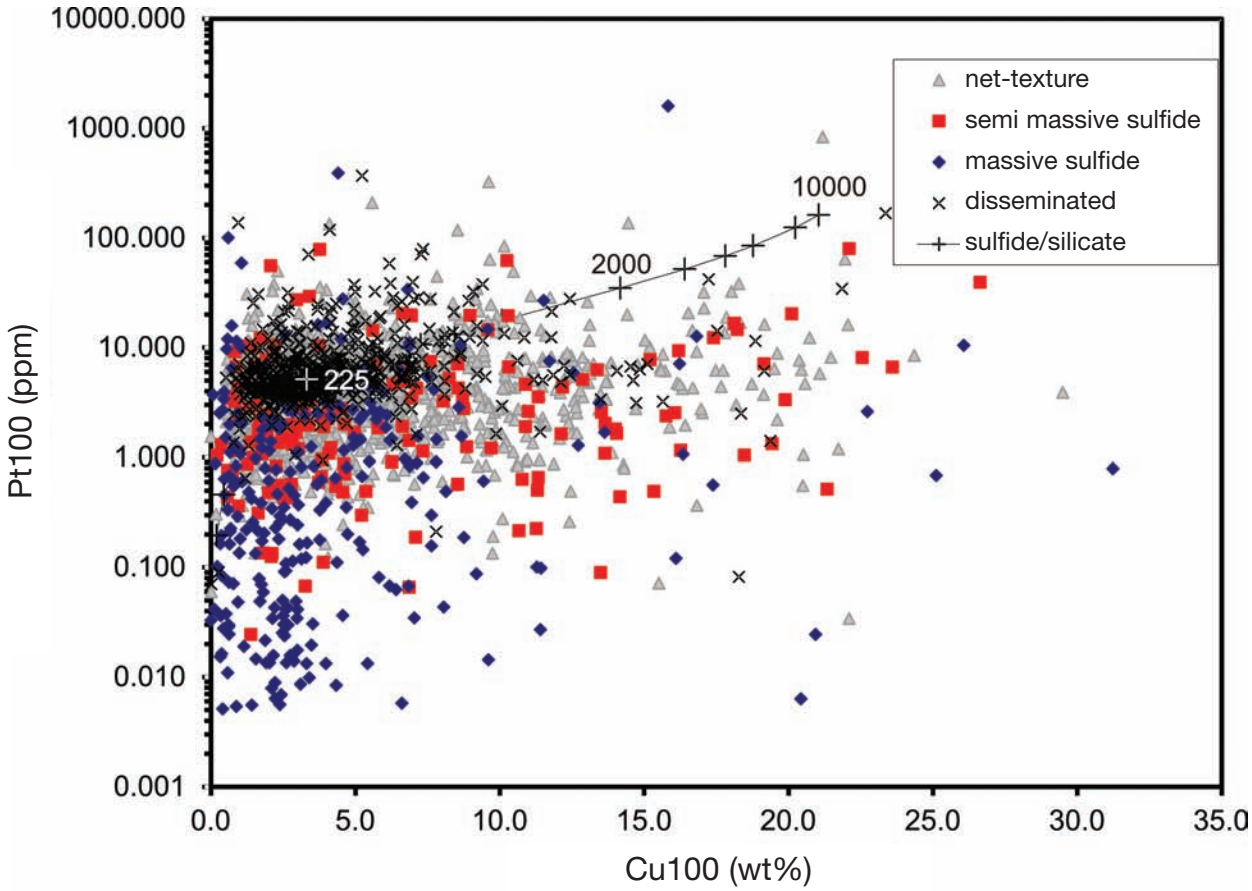

FIG. 10. Variation of Pt100 versus Cu100 for mineralized samples from the Eagle's Nest deposit. Symbols are as in Figure 9.

The distribution of pyrrhotite-rich domains tends to follow the massive and net-textured sulfide domains (Fig. 6), whereas the samples lowest in pyrrhotite and representative of migrating residual sulfide liquids tend to be concentrated along the margins of the intrusion and in discrete zones. Such zones are commonly recognizable in drill core as veins and masses of chalcopyrite-rich sulfide, which either cross-cut or replace pre-existing massive or net-textured sulfide, or which form separate Cu-rich veins within the silicate host rocks. These zones are of great potential importance because they might point to locations where late sulfide melt has drained out of the main ore zone into discrete and perhaps quite narrow pathways, such as brittle fracture systems. The existence of intrusive igneous breccias within the main dike attests to continued reactivation of the controlling fault structure and indicates that open dilatant pathways are likely to have existed, whereas late-stage sulfide liquids remained mobile even after the silicate intrusion may have completely solidified.

Conclusions

The Eagle's Nest magmatic sulfide deposit is a multimillion-tonne, polymetallic deposit with impressive grades of Ni, Cu, Pt, and Pd. It is hosted by a rather small Neoarchean ultramafic dike cutting slightly older granitoid intrusions immediately below a regional unconformity at the base of a major pile of metasedimentary and metavolcanic rocks. The dike that hosts the deposit appears to represent the lowest preserved structural level of a complex of ultramafic dikes and sills feeding into a layered intrusion several kilometers in diameter, which in turn underlies a volcanic pile of the same age. There is a remarkable concentration of mineral deposit types already known to exist within this Ring of Fire complex, including the Eagle's Nest magmatic sulfide deposit, several world-class chromitite deposits, a very large V-Ti-Fe deposit, and several VMS deposits.

The Eagle's Nest sulfides were generated by the assimilation of some combination of granodioritic and metasedimentary country rocks into a mantle-derived komatiite magma. The resulting slurry of olivine and metal-rich sulfide melt accumulated at the base of the dike to form an essentially continuous ribbon of massive and net-textured sulfides along a lateral extent of at least 1,000 m. After regional deformation, this structure now plunges vertically from outcrop to more than 1,000 m below surface.

Although much of the compositional variation within the Eagle's Nest deposit can be attributed to evolution of the sulfide magma through crystallization of mss and iss, there has been very substantial remobilization of Pt, most likely during metamorphism. Identification of zones where remobilized Pt has been redeposited could be of great economic significance.

The Ring of Fire complex has gone from being completely unrecognized to becoming one of Canada's most important emerging exploration and mining camps in only seven years. Much of the McFaulds Lake greenstone belt remains unexplored, allowing optimism that more important discoveries are still to be made.

REFERENCES

Armstrong, J.T., 1988, Quantitative analysis of silicates and oxide minerals: Comparison of Monte-Carlo, ZAF and Phi-Rho-Z procedures, *in* Newbury D.E., ed., Microbeam Analysis: San Francisco, California, San Francisco Press, p. 239–246.

Arndt, N., 2003, Komatiites, kimberlites, and boninites: Journal of Geophysical Research-Solid Earth, v. 108 B6, no. 11 p. 2293, doi: 10.1029/2002 JB002157.

Barnes, S.J., 1986, The effect of trapped liquid crystallization on cumulus mineral compositions in layered intrusions: Contributions to Mineralogy and Petrology, v. 93, p. 524–531.

——2007, Cotectic precipitation of olivine and sulfide liquid from komatiite magma and the origin of komatiite-hosted nickel sulfide mineralization at Mount Keith and Yakabinde, Western Australia: Economic Geology, v.102, p. 299–304.

Bennet, G., and Riley, R.A. 1969, Operation Lingman Lake: Ontario Department of Mines Miscellaneous Paper 27, 52 p.

Bostok, H.H., 1962, Geology Lansdowne House Ontario: Ontario Geological Survey Map 4-1962, scale one inch to four miles = 1:253 440.

Campbell, I.H., and Naldrett, A.J., 1979, Influence of silicate-sulfide ratios on the geochemistry of magmatic sulfides: Economic Geology, v.74, p. 1503–1506.

Cawthorn, R.G., Sander, B.K., and Jones, I.M., 1992, Evidence for the trapped liquid shift effect in the Mount Ayliff intrusion, South Africa: Contributions to Mineralogy and Petrology v. 111, p. 194–202.

Chung, H.-Y., and Mungall, J.E., 2009, Physical constraints on the migration of immiscible fluids through partially molten silicates, with special reference to magmatic sulfide ores: Earth and Planetary Science Letters, v. 286, p. 14–22.

Duffell, S., MacLaren, A.S., and Holman, R.H.C., 1963, Red Lake-Lansdowne House area, northwestern Ontario, Bedrock Geology, Geophysical and Geochemical Investigations: Geological Survey of Canada, Paper 63-5, 15 p. (Accompanied by Maps 2-1963, 3-1963, scale 1 inch to 8 miles)

Gao, S., Luo, T.C., Zhang, B.R., Zhang, H.F., Han, Y.W., Zhao, Z.D., and Hu, Y.K., 1998: Chemical composition of the continental crust as revealed by studies in East China: Geochimica et Cosmochimica Acta, v. 62, p. 1959–1975.

Golder Associates, 2010, Technical report and resource estimate, McFaulds Lake project, James Bay Lowlands, Ontario, Canada: Submitted to Noront Resources, April 23, 2010, 241 p.

Hart, S.R., and Davis, K.E., 1978, Nickel partitioning between olivine and silicate melt: Earth and Planetary Science Letters, v. 40, p. 203–219.

Henke, B.L., and Ebisu, E.A., 1974, Table of mass absorption coefficients: Advances in X-ray analysis, v. 17, p. 151–213.

Herzberg, C., and O'Hara, M.J., 1998, Phase equilibrium constraints on the origin of basalts, picrites, and komatiites: Earth Science Reviews, v. 44, p. 39–79.

Krogh, T.E., 1973, Low-contamination method for hydrothermal decomposition of zircon and extraction of U and Pb for isotopic age determinations: Geochimica et Cosmochimica Acta, v. 37, p. 485–494.

Krogh, T.E., 1982, Improved accuracy of U-Pb ages by the creation of more concordant systems using an air-abrasion techique: Geochimica et Cosmochimica Acta, v. 46, p. 637–649.

Lesher, C.M., and Keays, R.R., 2002, Komatiite-associated Ni-Cu-PGE deposits: Geology, mineralogy, geochemistry, and genesis: *in* Cabri, L.J., ed, The Geology, geochemistry, mineralogy and mineral beneficiation of platinum-group elements, CIM Special Volume 54, p. 579–618.

Li, C., Ripley, E.M., and Mathez, E.A., 2003, The effect of S on the partitioning of Ni between olivine and silicate melt in MORB: Chemical Geology, v. 201, p. 295–306.

Mavrogenes, J.A., and O'Neill, H.St.C., 1999, The relative effects of pressure, temperature and oxygen fugacity on the solubility of sulfide in natural magmas: Geochimica et Cosmochimica Acta, v. 63, p. 1173–1180.

McDonough, W.F., and Sun, S.S., 1995, The composition of the Earth: Chemical Geology, v. 120, p. 223–253.

Mungall, J.E., 2005, Magmatic geochemistry of the platinum-group elements, *in* Mungall, J.E., ed., Exploration for platinum-group element deposits, Mineralogical Association of Canada Short Course 35, p. 1–34.

——2007a, Crystallization of magmatic sulfides: An empirical model and application to Sudbury ores: Geochimica et Cosmochimica Acta, v. 71, p. 2809–2819.

——2007b, Crustal contamination of picritic magmas during transport through dikes: the Expo intrusive suite, Cape Smith fold belt, New Quebec: Journal of Petrology, v. 48, p. 1021–1039.

Naldrett, A.J., 2004, Magmatic sulfide deposits: Geology, geochemistry and exploration: New York, Springer, 728 p.

Percival, J.A., Sanborn-Barrie, M., Skulski, T., Stott, G.M., Helmstaedt, H., and White, D.J., 2006, Tectonic evolution of the western Superior province from NATMAP and lithoprobe studies: Canadian Journal of Earth Science, v. 43, p. 1085–1117.

Percival, J.A., Breaks, F.W., Brown, J.L., Corkery, M.T., Devaney, J., Dubé, B., McNicoll, V., Parker, J.R., Rogers, N., Sanborn-Barrie, M., Sasseville, C., Skulski, T., Stone, D., Stott, G.M., Syme, E.C., Thurston, P.C., Tomlinson, K.Y., and Whalen, J.B., 1999, Project 95034. Evolution of Archean continental and oceanic domains in the Western Superior province: 1999 NATMAP results: Ontario Geological Survey Open File Report 6000, Summary of Field Work and Other Activities 1999, p. 17-1–17-16.

Rayner, N., and Stott, G.M., 2005, Discrimination of Archean domains in the Sachigo subprovince: A progress report on the geochronology: Summary of field work and other activities 2005, Ontario Geological Survey, Open File Report 6172, p. 10-1–10-21.

Roeder, P.L., and Emslie, R.F., 1970, Olivine-liquid equilibrium: Contributions to Mineralogy and Petrology, v. 29, p. 275–289.

Seat, Z., Beresford, S.W., Grguric, B.A., Waugh, R.S., Hronsky, J.M.A., Gee, M.A.M., and Mathison, C.I., 2007, Architecture and emplacement of the Nebo-Babel gabbronorite-hosted magmatic Ni-Cu-PGE sulphide deposit, West Musgrave, Western Australia: Mineralium Deposita, v. 42, p. 551–581.

Seat, Z., Beresford, S.W., Grguric, B.A., Gee, M.A.M., and Grassineau, N.V., 2009, Re-evaluation of the role of external sulfur addition in the genesis of Ni-Cu-PGE deposits: Evidence from the Nebo-Babel Ni-Cu-PGE deposit, West Musgrave, Western Australia: Economic Geology, v. 104, p. 521–538.

Theyer, P., 1991, Petrography, chemistry and distribution of platinum and palladium in ultramafic rocks of the Bird River Sill, SE Manitoba, Canada: Mineralium Deposita v. 26, p. 165–174.

Thurston, P.C., Sage, R.P., and Siragusa, G.M., 1971a, Operation Winisk Lake: Winiskis Channel sheet. District of Kenora (Patricia Portion): Ontario Department of Mines and Northern Affairs, Preliminary Map P.0714, scale 1 inch to 2 miles.

——1971b, Operation Winisk Lake: Winisk Lake sheet. District of Kenora (Patricia Portion): Ontario Department of Mines and Northern Affairs, Preliminary Map P.0716, scale 1 inch to 2 miles.

——1979, Geology of the Winisk Lake area, district of Kenora, Patricia Portion; Ontario Geological Survey Report 193, 169 p. (With appendix by RA Riley). Accompanied by Maps 2287 and 2292, scale 1:253 440, and colored charts A and B.

Thurston, P.C., Osmani, I.A., and Stone, D., 1991, Northwestern Superior Province: Review and terrane analysis, *in* Thurston, H.R., eds., Geology of Ontario: Ontario Geological Survey, Special Vol. 4, Part 1, p. 81–144.

Timmins, E.A., Turek, A., and Symons, D.T.A., U-Pb zircon geochronology and paleomagnetism of the Bird River greenstone belt, Manitoba: Geological Society of Canada/Mineralogical Association of Canada Program with Abstracts 10, A-62.

TABLE A1. Isotopic Results

Analyte Symbol	Unit	DL	Analysis Method	NOT 09-2G12 73.6	NOT-07-10 78.5	NOT-08-36 256.7	NOT-08-36 226	NOT 07 17 33	model parent liquid	model contam-inant	NOT 07 17 33 ol	NOT 07 17 33 sp	NOT 07 17 33 opx
lithology				cm	gd	cm	omn	hz			n = 12	n = 2	n = 9
SiO_2	%	0.01	F-ICP	50.08	71.04	54.09	45.80	44.16	45.78	71.04	39.44	0.40	56.12
TiO_2	%	0.001	F-ICP	0.45	0.40	0.41	0.21	0.19	0.45	0.40	0.01	0.30	0.23
Al_2O_3	%	0.01	F-ICP	10.05	15.45	11.21	5.22	4.37	8.94	15.45	0.03	19.46	1.64
FeO*	%	0.01	F-ICP	10.00	2.02	8.25	11.33	11.42	11.64	2.02	16.41	37.37	8.41
MnO	%	0.001	F-ICP	0.18	0.03	0.16	0.18	0.18	0.21	0.03			0.21
MgO	%	0.01	F-ICP	18.56	1.51	13.68	32.61	34.90	22.05	1.51	44.26	4.67	31.62
CaO	%	0.01	F-ICP	7.28	1.98	7.19	3.13	2.84	8.36	1.98			1.88
Na_2O	%	0.01	F-ICP	1.35	5.64	3.46	0.20	0.45	0.47	5.64			
K_2O	%	0.01	F-ICP	0.91	1.60	0.52	0.03	0.17	0.77	1.60			0.00
P_2O_5	%	0.01	F-ICP	0.03	0.10	0.09	0.02	0.03	0.02	0.10			
LOI	%		F-ICP	2.39	1.16	2.40	8.21	7.14					
Sc	ppm	1	F-ICP	27	3	22	17	14					
V	ppm	5	F-MS	176	40	119	96	98	204	40	49	1620	
Cr	ppm	20	F-MS	2236	51	1256	3643	4832	2683	51	414	256708	4267
Co	ppm	1	F-MS	79	8	52	111	168	93	8			
Ni	ppm	20	F-MS	673	81	419	1365	2914	794	81	2273	769	609
Cu	ppm	10	F-MS	135	30	52	88	54	156	30			
Rb	ppm	1	F-MS	26	39	14	2	5					
Sr	ppm	2	F-ICP	102	356	174	18	24					
Y	ppm	0.5	F-MS	11	16	14	5	5	10	16			
Zr	ppm	1	F-MS	51	185	73	23	20	23	185			
Nb	ppm	0.2	F-MS	2.6	8.5	3.2	0.7	0.6	1.1	10.0			
Ba	ppm	3	F-ICP	126	295	105	8	35					
La	ppm	0.05	F-MS	5.4	29.5	11.4	2.5	1.4	1.2	26.0			
Ce	ppm	0.05	F-MS	10.2	58.0	21.4	5.6	3.2	3.1	45.0			
Pr	ppm	0.01	F-MS	1.39	6.04	2.65	0.56	0.45					
Nd	ppm	0.05	F-MS	5.8	17.2	8.9	2.2	1.9	2.9	20.0			
Sm	ppm	0.01	F-MS	1.42	2.93	1.88	0.54	0.50	1.03	3.30			
Eu	ppm	0.005	F-MS	0.45	1.15	0.50	0.21	0.18	0.33	1.05			
Gd	ppm	0.01	F-MS	1.71	2.54	2.10	0.70	0.60					
Tb	ppm	0.01	F-MS	0.30	0.40	0.38	0.13	0.11	0.27	0.46			
Dy	ppm	0.01	F-MS	1.86	2.45	2.29	0.84	0.75					
Ho	ppm	0.01	F-MS	0.38	0.53	0.45	0.19	0.17					
Er	ppm	0.01	F-MS	1.12	1.72	1.30	0.58	0.53					
Tm	ppm	0.005	F-MS	0.18	0.29	0.19	0.09	0.08					
Yb	ppm	0.01	F-MS	1.15	1.90	1.24	0.55	0.48	1.00	1.90			
Lu	ppm	0.002	F-MS	0.16	0.28	0.20	0.08	0.07	0.14	0.28			
Hf	ppm	0.1	F-MS	1.1	4.6	1.8	0.6	0.5	0.6	3.8			
Ta	ppm	0.01	F-MS	0.27	0.58	0.30	0.03	0.04					
Th	ppm	0.05	F-MS	1.0	5.2	5.3	0.6	0.4	0.1	5.5			
U	ppm	0.01	F-MS	0.27	1.47	2.18	0.21	0.13	0.03	1.44			
Ir	ppb		NI-FA	< 1									
Ru	ppb		NI-FA	10									
Rh	ppb		NI-FA	2									
Pt	ppb		NI-FA	13									
Pd	ppb		NI-FA	30									
Au	ppb		NI-FA	5									